INTERNATIONAL UNION OF
PURE AND APPLIED CHEMISTRY

MACROMOLECULAR DIVISION
WORKING PARTY ON STRUCTURE AND PROPERTIES OF
COMMERCIAL POLYMERS

BASIC PARAMETERS, MELT RHEOLOGY, PROCESSING AND END-USE PROPERTIES OF THREE SIMILAR LOW DENSITY POLYETHYLENE SAMPLES

Prepared for publication by
JOACHIM MEISSNER
BASF AG, Mess- und Prüflaboratorium WHM, D-6700 Ludwigshafen a.R., GFR

LONDON

BUTTERWORTHS

MACROMOLECULAR DIVISION

BASIC PARAMETERS, MELT RHEOLOGY, PROCESSING AND END-USE PROPERTIES OF THREE SIMILAR LOW DENSITY POLYETHYLENE SAMPLES

Prepared for publication by
JOACHIM MEISSNER
BASF AG, Mess- und Prüflaboratorium WHM, D-6700 Ludwigshafen a.R., GFR

SUMMARY

Participants from six laboratories have collaborated in a comprehensive study of three LDPE samples A, B, C (all of melt index 1.5) which are indistinguishable on the basis of measurements of melt index at 190°C, intrinsic viscosity, and GPC. The samples exhibit significant differences in processing (maximum drawdown speed in film blowing) and end-use properties (optical quality of blown film).

Rheological measurements have been made on the molten polymers at 150°C. The three samples show substantially the same linear viscoelastic behaviour (within limits of ±10 per cent) in oscillatory shear, in stress growth at the start of constant shear rate flow, and in stress relaxation, and have identical flow curves (viscosity versus shear rate). The three samples show differences in non-linear viscoelastic behaviour. In shear, these differences (in end correction, extrudate swell, and first normal stress difference) are associated primarily with the elastic part of the melt deformation, and are more pronounced at the lower shear rates (0.01–0.1 s^{-1}). The melt index values at 125°C are different for A, B and C. In elongation, the stress strain diagrams for A, B, C show significant differences if the elongation rate is low enough (0.01–0.1 s^{-1}) and the elongation strain is high enough. Flow birefringence has been measured in the transient region following the start of constant shear rate.

An important conclusion of this work is that, for the particular LDPE samples chosen, there are substantial differences in processing behaviour and end-use properties of blown film which are reflected in certain non-linear elastic properties of the melts but not in the results of characterization tests as commonly performed. The samples lie in the same order A, B, C for (1) increasing values of the critical drawdown speed (limited by bubble rupture in film blowing) and (2) of the optical quality of blown film (decreasing haze); (3) decreasing elastic contributions to the behaviour in shear flow; and (4) decreasing tensile stress in elongational flow (at low rates and large strains).

INTRODUCTION

In the relationships between basic parameters of polymers and end-use properties, polymer melt rheology is an important link. Consequently, the IUPAC Working Party on 'Structure and Properties of Commerical Polymers' has developed a strong activity in this field of research.

In a first collaborative test programme, six very different polymers were investigated with respect to the rheological behaviour of their melts by means of simple shear flow, oscillatory shear, and stress relaxation after cessation of steady shear flow[1]. The results of this first test programme show that there are remarkable differences between the (very) different polymer melts, and also that there is not always agreement if the same measurement is performed by several participating laboratories. The most important result of the first test programme, however, is the proof that rheologists from different countries and from competing companies can in fact cooperate and contribute to the progress in their field of interest.

The present, second test programme of the rheology subgroup of the IUPAC Working Party was formulated in 1967. This test programme for the first time attempts to connect technological as well as molecular characterization data, processing and end-use data with polymer melt rheology for low density polyethylene samples, which seem to be 'practically equal' according to the usual characterization methods. Additionally, this programme shows the need for:

(*a*) higher precision and accuracy of melt rheology measurements,
(*b*) further improvements of the existing experimental tools,
(*c*) completely new measuring devices.

For this test programme, three samples of low density polyethylene (LDPE) were selected, which are similar in chemical characterization and also in the viscous flow behaviour of the melts but which are different in some distinct processing and end-use properties. These differences are mainly found in film blowing and in the final properties of the blown films. The samples were supplied by BASF Aktiengesellschaft, Ludwigshafen am Rhein, Germany. They are designated in the following by A, B and C*.

The test programme includes measurements in polymer melt rheology of practically every kind available at present, always with the same samples. This makes the test results especially interesting. The presentation of these results corresponds to the test programme with the following main topics:

(A) General Data and Molecular Characterization,
(B) Processing Properties and End-use Data,
(C) Polymer Melt Rheology,
  (C1) Linear Viscoelastic Behaviour,
  (C2) Viscosity Function in the Non-linear Range,
  (C3) Elastic Effects in Extrusion Flow.
  (C4) Rheological Studies with Cone-and-plate Rheometers,
  (C5) Tensile Flow Properties,
(D) Final Results and Conclusions of the Collaborative Study.

The following laboratories participated in the experimental work:

(I) Monsanto, Fawley, Great Britain, and Texas City, USA,
(II) Rhône-Progil, Antony, France,
(III) Solvay, Brussels, Belgium,
(IV) BASF, Ludwigshafen am Rhein, GFR,
(V) Industrial Chemistry Institute, Warsaw, Poland,
(VI) Central Laboratory TNO, Delft, Netherlands.

* It should be noted that the samples A and B are different from the samples LDPE-A and -B of the former report[1].

For convenience, henceforth the above laboratories will be referred to by the Roman numerals given above. In order to condense the presentation, only brief experimental details are given.

(A) GENERAL DATA AND MOLECULAR CHARACTERIZATION

In this section, those data are given which are generally used for the characterization of polyethylene. Density (at room temperature) and melt index classify the different types of polyethylene. Melt memory index is often used in the plastics industry for an estimate of 'the elasticity' of the melt. Infra-red measurements give a determination of the (short) side groups of the polyethylene molecule.

The intrinsic viscosity $[\eta]$ and the gel permeation chromatography (GPC) method give molecular parameters from the behaviour of the polymer in a very dilute solution. In this field, open questions concerning the test method and the evaluation of the data still exist. To solve these problems, a new IUPAC Working Party on Molecular Characterization of Commerical Polymers was formed in 1968. Currently, this group is involved in a more detailed molecular characterization study of the samples A, B, C. Therefore, with regard to this item, only preliminary results can be reported.

In addition, results concerning the thermal stability of the melts are included in this section. Important consequences follow for the temperature range at which melt rheology measurements should be performed in order to avoid changes of the structure of the bulk material because of chemical reactions in the melt[2].

(A1) Density

The density of the samples A, B, C at room temperature is given in *Table 1* together with a short description of the methods used and the pre-treatment of the specimens. The data reflect the well-known influence of the specimen preparation. Under comparable conditions (line 3 and line 6 of the table), the density of the three samples at 20°C after annealing at 100°C is $\rho(20°C) = 0.919 \pm 0.001$ g/cm^3.

From *Table 1* it follows that, independent of the conditions and methods used, the densities of A and C coincide and that in all cases the density of sample B is slightly higher. The difference in density between B and A or C is of the order of 0.001.

(A2) Melt flow index

The melt flow index (MFI) is internationally used for the grading of polyethylene and also of other polymers. For the measurement of the MFI, all the participants used the same conditions defined in ASTM or DIN standards*.

* In addition, participant I reported data for the much lower temperature of 125°C and 8.6 kgf piston load. The data (in g/10 min) for sample A are: 1.35; B: 1.99; C: 2.45. The data show that differences between the three samples appear if the melt flow index is measured at lower temperatures. This result has been confirmed by other participants too, and will be discussed in section C3.

Table 1. Density at room temperature (different sources using different methods)

	Participant	Temperature [°C]	Method	Density of sample [g/cm³] A	B	C	Comment
(1)	I	23	ASTM D 792–50[a]	0.9170	0.9180	0.9170	'nominal density'[b]
(2)	I	23	„	0.9200	0.9210	0.9201	'absolute density'[c]
(3)	I	20	calculated[d]	0.9188	0.9198	0.9188	'nominal density'[b]
(4)	I	20	from (1) and (2)	0.9218	0.9228	0.9219	'absolute density'[c]
(5)	III	20	ASTM D 1505[e]	0.918	0.919	0.918	
(6)	IV	20	DIN 53 479 Sect. 7.2[f]	0.9182	0.9198	0.9184	[g]

[a] displacement of a like volume of liquid.
[b] density obtained after annealing at 100°C.
[c] slow cooling from 150°C to room temperature over 24 h.
[d] density of polyethylene decreases approximately by 0.0006 g/cm³ for every 1°C rise in temperature over the range 20 to 23°C, see Note 1 of reference 3.
[e] density grandient.
[f] buoyancy in methanol.
[g] specimens are pre-tempered at 100°C for 1 h, then cooled in air.

Table 2. Melt flow index (*ASTM D 1238*, *BS 2782*, Method 105 C, or *DIN 53 735*)
Standard conditions (Melt temperature 190°C, piston load 2.16 kgf)

Participant	Melt flow index [g/10 min] A	B	C
I	1.33	1.38	1.56
III	1.4	1.4	1.6
IV	1.39	1.44	1.62
V	1.36	1.42	1.56
Average	1.37	1.41	1.59

The data are given in *Table 2*. Considering the usual scatter of MFI measurements, it follows from this table that:

(*a*) for each sample the results of the different participants are in excellent agreement;

(*b*) samples A and B show the same MFI, whereas the MFI of sample C is slightly higher. For A or B the result is MFI = 1.4 compared with MFI = 1.6 for sample C;

(*c*) the largest difference between the averages of the MFI of the three samples exists between samples A and C and has a magnitude of 15 per cent.

(A3) Melt memory index

Melt memory index or, more precisely, the extrudate swell of the melt flowing out of the die of the melt indexer (compare section A2) is widely used

in industry as a quick indication of melt elasticity. However, this practice does not give reasonable physical information because (among other reasons) the diameter is determined after cooling the extrudate in air, so that the equilibrium swell is not obtained.

Table 3. Melt memory index (Extrudate swell ratio $(d - d_0)/d_0$ [per cent] using the melt indexer, compare section A2. Melt temperature 190°C, piston load 2.16 kgf, d is the extrudate diameter, d_0 is the die diameter 2.095 mm. All extrudate specimens cooled in air)

Participant	A	B	C	Comment
I	51.5	52.7	47.9	[a]
IV	49	51	45	[b]
IV	54	55	48	[c]
V	54	59	53	[d]

[a] Cut-off specimen of 10 cm length; diameter measured as a function of specimen length and extrapolated to length zero.
[b] measured at 15 mm distance from first cut-off surface.
[c] average diameter of thickest part of cut-off.
[d] average of *ca.* 30 diameter determinations of 20 mm long cut-offs collected during MFI determination.

The data with details of the measuring technique are given in *Table 3*. Because of the undefined thermal history, the different participants obtain different absolute values. However, it seems to be remarkable that (at 190°C) the order of the memory data for the three samples is the same for all participants: A and B very closely have the same melt memory index (for B slightly higher than for A), whereas for C the values are smaller* (Exception: Data of V gave a distinctly higher melt memory for B than for A or C).

(A4) Infra-red absorption

The results of the infra-red studies are shown in *Table 4*. Considering the normal scatter of the data, the following comparison between samples A, B, C can be made: (a) the number of methyl groups is equal for A, B, C (except for the results of V), (b) all participants agree that sample B has definitely more vinyl groups than A or C which are equal in vinyl groups; (c) the number of vinylidene groups is very similar for A, B, and C; (d) III and IVa give *trans* data which are opposite with respect to the order of A, B, C.

Hence, with the exception of the vinyl groups, the i.r. data are similar for A, B, C. Concerning the absolute values, however, remarkable differences exist between the different participants. But the main subject here is the comparison of samples A, B, C. The difficulties of the absolute characterization of the branched polyethylene molecule have led to the creation of another Working Party of the Macromolecular Division of IUPAC, and it should be noted that this new Working Party on 'Molecular Characterization of Commercial Polymers' has distributed the samples A, B, C to many more

* The additional melt memory index data of participant I at 125°C and 8.6 kgf piston load (compare footnote on page 555 are for sample A: 51.5; B: 49.1; C: 44.2 per cent. Under these conditions, sample A has a higher melt memory than B which is in contrast to the results at 190°C.

Table 4. Infra-red absorption data (IVa and IVb correspond to two different laboratories of IV)

	Participant	A	B	C
$-CH_3$/1000 C (methyl)	III	14	15	15
	IVa	31	31	31
	IVb	34	34	34
	V	22.7	20.5	24.1
$-CH=CH_2$/1000 C (vinyl)	III	0.06	0.12	0.05
	IVa	0.08	0.14	0.10
	IVb	0.11	0.18	0.08
$R-\overset{\displaystyle CH_2}{\overset{\|}{C}}-R$/1000 C (vinylidene)	III	0.51	0.44	0.51
	IVa	0.68	0.58	0.69
	IVb	0.7	0.6	0.6
$-CH=CH-$/1000 C (*trans*)	III	0.07	0.07	0.09
	IVa	0.13	0.09	0.10
	IVb	0.10	0.09	0.10

laboratories. The average values and the scatter obtained from these additional measurements were published recently[4].

(A5) Intrinsic viscosity

Results for the intrinsic viscosity of the three samples in different solvents and at different temperatures are given in *Table 5*. More data for the same samples have been reported by Strazielle and Benoit[4]. According to the latter report, data obtained under the same conditions in four different laboratories did not differ by more than ten per cent. It may be concluded, therefore, that within experimental accuracy, no difference exists between the three samples as far as intrinsic viscosity is concerned.

Table 5. Intrinsic viscosity $[\eta]$ in dl/g

Participant	Exptl condition	A	B	C
I	*p*-Xylene, 105°C	0.89	0.87	0.89
III	Tetralin, 160°C	1.0	1.0	1.0
IV	Decalin, 130°C	1.10	1.12	1.08

(A6) Light scattering and gel permeation chromatography

Molecular characterization of branched polymers by means of the GPC technique is still in its infancy and is subject to erroneous interpretations[4]. GPC traces for the three LDPE samples obtained by nine different laboratories participating in the IUPAC Working Party on Molecular Characterization of Commercial Polymers[5] show, in general, rather slight differences, which may induce one to conclude that the three samples have very similar

molecular size distributions. An example of the results obtained by IV is given in *Figure 1*.

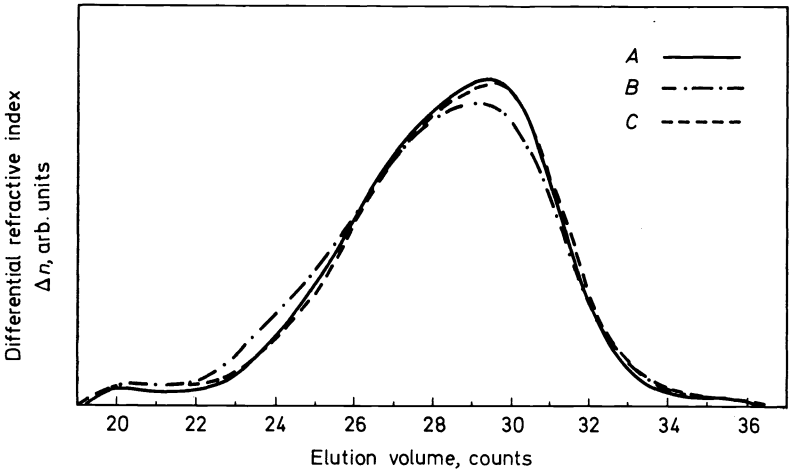

Figure 1. Results of gel permeation chromatography for the determination of molecular weight distribution; from IV (Dr Ball).

Light-scattering measurements by seven different laboratories seem, however, to indicate that the three samples have appreciably different weight-average molecular weights[5]. Sample B has an M_w value of the order of 6×10^5, sample C a somewhat higher one ($8–9 \times 10^5$), and the value for sample A is apparently still higher ($> 10^6$). Light scattering measurements on sample A are not very accurate because of the presence of a small amount of microgel, which markedly affects the calculated value for M_w. This may explain why the discrepancy between the values obtained by different laboratories is more important for sample A than for the other samples. Number-average molecular weights obtained in different laboratories by means of various methods[4,5] are very similar for the three samples and are of the order of 2×10^4.

In conclusion, our knowledge of the molecular characteristics of the three LDPE samples is still unsatisfactory and reflects the general situation in the field of branched polymers. It is hoped that further work by the IUPAC Working Party on Molecular Characterization of Commercial Polymers will lead to the development of more accurate and more reliable methods of analysis by means of dilute solution techniques.

(A7) Thermal stability of the melts

In order to obtain reliable and significant results from polymer melt rheology, the melts must have a sufficient thermal stability under the test conditions. This is especially important if the temperature dependence of rheological properties is to be measured, and different types of experimental equipment (requiring different residence times before the physical measurements can

start) are to be used. Molecular reactions in the melt, due to temperature and duration of the measurement, may change the rheological properties, as has been demonstrated for HDPE[2] as well as for LDPE[6]. For the stability check, three types of measurement were used:

Ia: In DTA, the times required (at 130 and 190°C) for noticeable chemical reactions to occur were determined. This test was performed with sample A, 'as received' and 'stabilized'. The results of *Table 6*—(Ia) indicate that at 130°C the sample is stable during the time of a rheological measurement, whether the sample is 'stabilized' or not. However, this is not so at 190°C.

Table 6. Thermal stability of the melts

(Ia) Time for the occurrence of a chemical reaction in DTA (formation of hydroperoxides?)

		130	190°C
sample A,	'as received'	1400	12 min
	stabilized	2400	6 min

(Ib) Zero shear viscosity, η_0 at 190°C*

	A	B	C
'as received'	1.67	1.78	2.5×10^5 Poise
stabilized	1.26	1.37	1.26

* for more data concerning η_0 reference may be made to section C.

Ib: In the second test, the zero shear viscosity η_0 of the melt was measured at 190°C in the Weissenberg rheogoniometer (WRG). The detailed discussion of the rheological aspects is made in section C. Here, the difference between the 'as received' samples and the stabilized ones matters, compare *Table 6*—(Ib).

IV: The melt indexer (compare section A2) is used at 150°C with 5 kgf piston load. Each specimen was pre-tempered at different temperatures T under vacuum for 30 min. The output rate in the melt indexer under these conditions is shown in *Figure 2* as a function of the temperature of the thermal pre-treatment. In addition, the results for the 'as received' samples are given.

On the average, rheological measurements on the melt last about 30 min (including pre-heating of the samples in the apparatus). Therefore, *Figure 2* gives a good indication of the stability of the melt during that period of time at different temperatures. It follows from *Figure 2* that results at $T > 170$°C do not reflect the properties of the 'as received' samples; and, even at $T < 170$°C, the results for B and C differ from the 'as received' samples, whereas—and this is a remarkable result—sample A seems to be unchanged. Significant differences for 'as received' samples (MFI at 150°C) are consistent with similar results at 125°C already noted (footnote page 555).

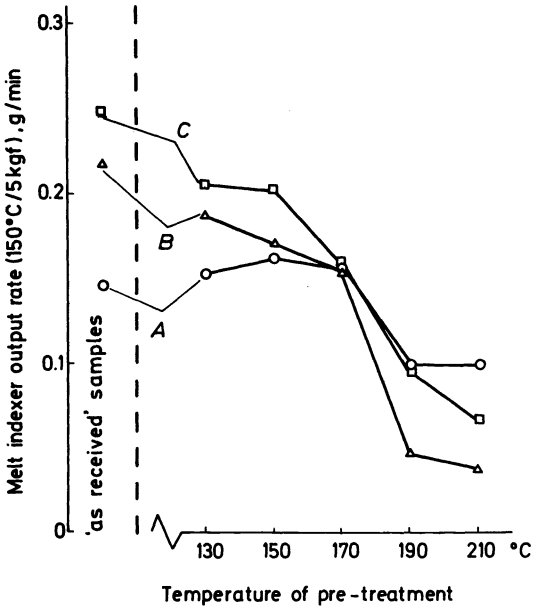

Figure 2. Stability of LDPE samples A, B, C. Melt indexer output rate of specimens which were pre-heated for 30 min under vacuum at different temperatures. The abscissa indicates the temperature of this pre-treatment. The melt indexer output rate is measured at 150°C and 5 kgf piston load.

(A8) Conclusions of section A

The three samples A, B, C *are equal* in:

(1) density (at 20°C after annealing at $T = 100$°C; $\rho = 0.919 \pm 0.001$ g/cm^3),

(2) melt index (MFI $= 1.5 \pm 0.1$),

(3) i.r. data: (a) methyl groups, (b) vinylidene groups, (c) *trans* double bonds,

(4) intrinsic viscosity $[\eta]$,

(5) number-average molecular weight M_n.

A, B, C *seem to be different* in:

(1) weight-average molecular weight M_w, by light scattering. A seems to have a higher M_w than B or C;

(2) molecular weight distribution.

A. B, C *are different* in:

(1) melt memory index: sample C shows a smaller memory than A or B. However, the difference in melt memory is rather small;

(2) i.r. data: B has more vinyl groups than A or C;

(3) thermal stability of the melt, especially for $T > 170$°C.

This summary shows as a first conclusion that the requirements of the original plan are fulfilled, viz. to select LDPE samples which are similar or even equal with respect to the usual characterization of LDPE. However, in

spite of the agreement of these 'fundamental parameters', one cannot treat the samples as being identical because there are remarkable differences in some processing and end-use data as will be shown in the next section. Hence, the somewhat disappointing second conclusion has to be that, at present, neither the technological standard characterization nor the characterization by means of the macromolecular physical chemistry of the dilute solution can reflect the differences which are found in some processing and end-use properties of the LDPE samples under test.

(B) PROCESSING PROPERTIES AND END-USE DATA

In selecting the samples for the present test programme, differences between samples A, B, C in film blowing and in the properties of the blown film were detected. Therefore, it is the behaviour in film blowing which is chosen to characterize the processing behaviour; and, in the main, it is the mechanical and optical properties of blown film which are used to characterize end-use data. In film blowing, the critical technological quantity is the maximum production speed which is governed by the maximum film drawdown. If the drawdown speed is increased beyond this critical value, failure of the bubble occurs. For the determination of differences in film blowing and in the properties of the blown films, great care was taken to ensure that the conditions of film blowing as well as extrusion were equal for A, B, C. Thus, comparable films were obtained for the three samples.

(B1) Film drawdown

There is no standard for the determination of the critical drawdown speed at which failure of the bubble occurs. Therefore, the two participating laboratories used different extrusion and blow conditions:

(I) 2.5 in. extruder, 6 in. diameter film die, 1 mm gap, screw speed 35 rev/min, blow ratio (ratio bubble diameter: die diameter) 2:1.

(IV) Reifenhäuser extruder S45, 45 mm screw diameter, $L = 20\,D$, 50 mm diameter film die, gap 0.5 mm. Screw speed 22 rev/min, blow ratio 2:1. Constant length of the neck (distance die exit–freezing zone) maintained by adjusting the cooling air. The take-off speed is increased in steps*. If the bubble is stable for ten minutes, the next higher take-off speed is used. A different take-off speed results in a different film thickness because the screw speed is kept constant.

In *Table 7* the critical drawdown speeds are given together with the corresponding film thicknesses at break. The data show that there are remarkable differences in the maximum production speed for A, B, C. Sample A always has the lowest, and C the highest, critical drawdown speed. Correspondingly, the film thickness at break of C is the smallest, and that of A the highest.

* It should be noted that production equipment for film blowing often does not allow a continuous, but only a stepwise, change of the drawdown speed. Therefore, the 'critical' drawdown speed cannot be determined as accurately as one would like. This disadvantage often occurs with 'processing data', and it is necessary that in this respect improvements are made in future test programmes.

Table 7. Critical film drawdown and corresponding film thickness at break

Participant	Melt temp.		A	B	C	Comments
I	180°C	critical film drawdown	49	52	62 m/min	[a]
		film thickness at break	13	9	6 μm	[b]
IV	180°C	critical film drawdown	18	23	23 m/min	[c]
		film thickness at break	15	10	10 μm	[d]
IV	150°C	critical film drawdown	13	23	23 m/min	[c]
		film thickness at break	20	10	10 μm	[d]

[a] Best results from three runs quoted.
[b] Failure of the bubble caused (A) by 'oxidized material', (B) by 'fine, hard gel', (C) by 'small gel'.
[c] The drawdown equipment was changed only in steps of 7–11–13–18–23 m/min, compare footnote on page 562.
[d] Film thickness and drawdown speed are related to each other because the extruder screw speed was kept constant.

With respect to B, the two participants report apparently opposite behaviour. I finds that B behaves like A, whereas IV finds that B behaves like C. According to IV, the difference between A and B or C is more pronounced at 150°C than at 180°C.

(B2) Mechanical properties of blown film

The tests for the determination of the mechanical properties of the blown

Table 8. Results of tensile tests of blown film at room temperature

Participant	Deformation rate*		A	B	C
		Film thickness	38	38	38 μm
I	500 mm/min	yield strength	201	208	197 kgf/cm²[a, b]
		rupture strength	273	252	259 kgf/cm²
		rupture strain	670	640	635%
		5% secant modulus	1.810	2.060	2.080 kgf/cm²
		Film thickness	115	104	114 μm
III	500 mm/min	yield strength	80.0	82.8	76.5 kgf/cm²[c]
		rupture strength	149	148	147 kgf/cm²
		rupture strain	588	528	570%
	50 mm/min	yield strength	72.6	73.8	70.2 kgf/cm²
		rupture strength	140	139	139 kgf/cm²
		rupture strain	556	505	554%
	5 mm/min	yield strength	63.8	60.9	61.3 kgf/cm²
		rupture strength	122	114	129 kgf/cm²
		rupture strain	517	455	530%

* Deformation rate here means crosshead speed of the tensile testing machine.
[a] *ASTM D 822-61 T:* Tensile properties of thin plastic sheeting.
[b] Mean value obtained in longitudinal and transverse directions.
[c] *DIN 53 455:* Zugversuch, 100 mm initial crosshead separation, longitudinal direction (N.B. tensile deformation and drawdown in film blowing have the same direction).

film at room temperature can be subdivided into two groups: (a) performance in tensile tests, and (b) impact tests. The results are given in *Tables 8* and *9*. The absolute values for the different strength data of *Table 8* are different for the two participants; however, it is remarkable that with respect to A, B, C, each participant finds differences which are smaller than ten per cent, and in some cases much smaller than ten per cent. Therefore, the mechanical properties of the blown film measured in tensile tests are practically equal for A, B and C. This statement is not valid for the impact tests (*Table 9*). There are practically the same data if the impact deformation is in the longitudinal direction. But, in the transverse direction, both participants III and IV notice a much lower strength for material B than for A or C. The impact strength of A film in the transverse direction is about 25 per cent higher than that of B film, and 20 per cent (participant IV) or only 4 per cent (participant III) higher than that of C film*. The film drop dart impact test of participant I does not reflect this result, because the anisotropy of the film properties has no influence on the dart impact strength.

Table 9. Results of impact tests of blown film

Participant	Quantity	A	B	C	Method
I	Film thickness		38 μm		
	Film drop dart impact strength	142	146	144 gf	*ASTM D 1709–59 T*[a]
III	Film thickness	115	104	114 μm	
	Tearing strength				
	(a) longitudinal	3.77	3.95	4.66 kgf/mm	TAPPI Standard[b]
	(b) transverse	8.62	6.93	8.31 kgf/mm	*T 414 ts-64*
IV	Film thickness		40 μm		
	Tearing strength				
	(a) longitudinal	6.6	6.8	6.6 kgf	[c]
	(b) transverse	6.5	4.7	5.2 kgf	

[a] Impact resistance of PE film. A dart falls freely through a length of 66 cm and hits the film. The weight of the dart is changed until 50 per cent of the film specimens fail, in which case the weight corresponds to the 'impact strength'.

[b] A pendulum swings through an arc and tears the specimen of blown film from a pre-cut slit. The energy tearing the specimen is measured indicating also the tearing force because all specimens have the same length. In order to allow for the different film thickness, the data reported indicate the tearing force divided by film thickness.

[c] The film specimen is clamped in an arc of a circle at the centre of which a pendulum is fixed. The falling pendulum tears the specimen by means of a special knife at the pendulum head. The tearing strength being determined is the ratio of dissipated pendulum energy to the length of the tear produced by the knife.

(B3) Optical properties of blown film

In these properties again the absolute figures are of minor value because there do not exist procedures of film blowing and examination which are used in the same way by all participants; however, the comparison of the three samples is the vital point, and in this respect the optical properties of the blown film give pronounced differences, *Table 10*.

* This result of the impact tests shows that, for future similar test programmes, the anisotropy of the mechanical behaviour should be measured in the tensile tests also.

Both participants (I and IV) use the same terms to characterize the optical quality of the films: *Haze* is the percentage of transmitted light flux which in passing through the film specimen deviates from the incident beam by forward scattering with an angle of $\alpha > \alpha_0$. *Gloss* denotes the percentage of reflected light flux; a beam of light is incident at 45° and reflected at 45°; the reflected light is measured by a photocell and expressed as a percentage of the light reflected from a black standard (I: black tile, IV: black polished glass plate). *Clarity* is the amount of light which deviates less than four minutes of arc on transmission through the PE film; the result is expressed as a percentage of the light incident on the film.

Table 10. Optical properties of blown film

Participant	Film blowing	Film thickness		A	B	C
I	Usual procedure of I	38 μm	Haze	17.2	9.1	8.7% [a]
			Gloss	17.5	32.0	34.5%
			Clarity	6.9	38.2	39.5%
IV	Usual procedure of IV	40 μm	Haze	54	30	23% [b]
			Gloss	49	81	78 scales[c]
	Melt temperature 150°C	40 μm	Haze	62	23	22%
			Gloss	38	83	84 scales
		20 μm	Haze	73	32	28%
			Gloss	24	59	67 scales
	Melt temperature 180°C	40 μm	Haze	63	36	30%
			Gloss	42	73	78 scales
		20 μm	Haze	73	40	38%
			Gloss	29	57	61 scales

[a] *ASTM D 1003-61*, for definition of haze see text, participant I uses $\alpha_0 = 2.5°$.
[b] Compare comment (a), participant IV uses $\alpha_0 = 0.8°$.
[c] Gloss meter of Fa Lange, Berlin, is used. Standard is a polished glass plate with five per cent reflection which is adjusted to 100 scales.

The results of these tests can be expressed as follows. Both I and IV observe remarkable differences in optical properties. Sample A has much more haze and much less gloss than B or C*. Thus the optical properties of blown film from B or C are much better than those from A. The film blowing conditions have no influence on this statement. Samples B and C are very similar in their optical properties.

(B4) Conclusions of section B

There are in fact remarkable differences in processing and end-use behaviour between the three samples: especially in film drawdown and in the

* The haze of these thin films is predominantly an 'external' haze caused by surface roughness. As is well known, the optical properties are greatly improved as soon as the effects of surface roughness are eliminated, e.g. by immersion in paraffin or silicone oil[7].

optical properties of blown film, samples B and C are similar whereas sample A gives much poorer results. With respect to the mechanical properties of blown film, the three samples are, on the whole, alike, but there is one exception: in impact strength in the transverse direction, A shows the highest, and B the lowest, strength.

(C) POLYMER MELT RHEOLOGY

Polymer melt rheology is the main subject of this paper, and therefore rheological measurements of an extended variety were performed. The comprehensive data are interesting in themselves and will be given in the following in spite of the fact that the samples A, B, C do not differ much in many respects, e.g. in linear viscoelastic behaviour and viscous flow properties. However, this does not mean that there are no obvious differences to be shown in melt rheological properties at all. In the presentation of the data, we follow the main topics of the test programme given already in the introduction.

(C1) Linear viscoelastic behaviour

The linear viscoelastic properties were studied at sufficiently small values of total shear or shear rate. These studies include the determination of (1) the zero shear viscosity η_0 and its temperature dependence; (2) time-dependent, and (3) frequency-dependent linear viscoelastic material functions. Since the object of this study is the comparison of the properties of the three samples A, B, C, preference is given to the presentation of the directly measured material functions instead of a further evaluation of the data. This is the reason that the relaxation spectrum (for example) is not discussed here.

(C1.1) *Zero shear viscosity* η_0

At constant shear rate $\dot{\gamma}$ and sufficiently long duration of shear, the LDPE samples show an equilibrium shear stress p_{12} which is proportional to $\dot{\gamma}$, if $\dot{\gamma}$ is low enough. Thus, the quantity

$$\eta_0 = \lim_{\substack{\dot{\gamma}\to 0 \\ t\to\infty}} p_{12}(t,\dot{\gamma})/\dot{\gamma} \tag{1}$$

is a characteristic linear viscoelastic material constant which is called zero shear viscosity.

The measurements were performed with cone-and-plate viscometers. Participant I used the commercial version[8] of the Weissenberg rheogoniometer (WRG), model R 16; II used the Kepes cone-and-plate viscometer[9]; and IV used a modified version[10] of the WRG. In order to approach the limit in equation 1, the lowest shear rates possible were applied. However, the minimum shear rates differ considerably because of the different types of instruments and cone-and-plate diameters used. As an example of the test results, *Figure 3* shows the viscosity data calculated from the equilibrium shear stress at different temperatures for sample A. The horizontal parts of the curves correspond to η_0, and it follows from this figure that only the results of IV seem to approach this limit correctly. As follows from the caption of *Figure 3*, the much smaller minimum shear rate of IV was achieved by using

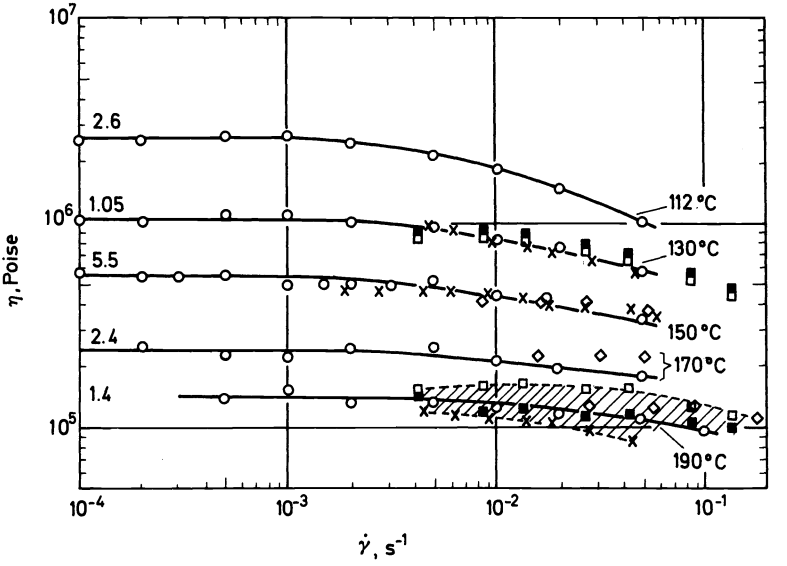

Figure 3. Determination of zero shear viscosity η_0; sample A. I: □ WRG (25 mm diameter, cone angle $\alpha = 4°$), ■ sample A stabilized, ◇ temperature shift of 130°C data using $E = 11.7$ kcal/mole[11]. II: × Kepes (26.15 mm diameter, $\alpha = 2° 14'$). IV: ○ WRG modified (72 mm diameter, $\alpha = 4°$).

relatively large cone-and-plate diameters. Participant I measured, at 130 and 190°C, 'as received' and stabilized material. Considering the scatter of the data, there is a sufficient coincidence of these data at 130°C, but pronounced differences at 190°C which reflect again the problem of thermal instability already discussed in item A7. In addition, I applied a temperature/shear rate shift treatment of his 130°C data to other temperatures[11].

The zero shear viscosities η_0 are tabulated in *Table 11*. At the lowest temperatures material C has the lowest η_0, which are about ten per cent smaller than those of A or B. A and B show practically the same results. This is also valid for 150°C according to IV. However, II reports at 150°C the opposite. The viscosity of C measured by II is slightly higher than that of A or B, which have again the same η_0. At 170 and 190°C, the three specimens cannot be compared because of the different thermal stability. At 130°C, I reports lower equilibrium viscosities than IV, but this is a consequence of the different experimental conditions. II does not obtain a horizontal level of the viscosity function for $\dot{\gamma} \to 0$ at 130 and 190°C. Therefore, data from II are listed in *Table 11* only for 150°C.

If $\log \eta_0$ is plotted as a function of $1/T$ (reciprocal absolute temperature), straight lines are obtained, as has been shown for a similar LDPE melt previously[12]. Apparently, the Arrhenius relation

$$\eta_0 \propto \exp(E_0/RT) \tag{2}$$

where E_0 is the activation constant, and R the gas constant, holds, and, from the slope of the straight line, E_0 can be determined. The data for E_0 are indicated in *Table 11* too. It follows that, within the experimental scatter, all

Table 11. Zero shear viscosity η_0 at different temperatures; activation constant E_0

Temp. °C	Participant	A	B	C
112	IV	26.0	26.3	24.0×10^5 Poise
130	Ia	8.3	9.5	8.4
130	Ib	9.4	†	8·0
130	IV	10.5	11.8	9.7
150	Ic	4.2	5.2	4.5
150	II	4.7	4.7	4.9
150	IV	5.5	5.5	5.0
170	Ic	2.2_5	2.7	2.5
170	IV	2.3_8	2.5_5	2.4_3
190	Ia	1.65	1.75	2.4
190	Ib	1.2_5	1.3_7	1.2_5
190	Ic	1.2_5	1.5_5	1.4
190	IV	1.4	‡	1.5_5
E_0	IV	13.8	13.5	13.4 kcal/mole

Ia: From direct measurement of I; Ib: stabilized material, Ic: 'shifting' of the 130°C results Ia[11].
† no results received; ‡ not measurable because torque increases continuously during the test due to chemical reactions.

three samples A, B, C have the same activation constant,

$$E_0 = 13.6 \pm 0.2 \text{ kcal/mole} \tag{3}$$

which coincides perfectly with the activation constants given for LDPE elsewhere[13]. In this context, the data of I cannot be considered, because (a) at 190°C they deviate too much from the data for the stabilized material, and (b) the data, obtained by shifting the 130°C results of I to other temperatures, make use of an *a priori* activation constant of $E_0 = 11.7$ kcal/mole in order to perform this shift[11]. This difference in E_0-values seems to be the reason for the deviation of the shifted and measured data of *Figure 3*.

During the test programme, an attempt was made to characterize the extent of the linear viscoelastic shear range by defining a limiting shear rate $\dot{\gamma}^*$ at which the measured viscosity $\eta(\dot{\gamma}^*) = 0.9\,\eta_0$. It turned out, however, that there were tremendous differences in $\dot{\gamma}^*$ between the different participants. This reflects the difficulty in determining correctly the location of the ten per cent deviation from η_0 of these very smoothly bent curves.

Comparing the three samples, the following conclusions can be drawn. Samples A, B, C have the same zero shear viscosity η_0 within a scatter of $\pm$ 10 per cent in the temperature range 112–170°C. The temperature dependence of η_0 is described by an Arrhenius relation; the activation constant E_0 shows no difference in magnitude between A, B, C, and coincides with data from the literature. From the experimental point of view, the results show that, for the determination of η_0, it is essential to operate in a low enough shear rate range.

(C1.2) *Time-dependent linear viscoelastic material functions*

In order to determine time-dependent linear viscoelastic material functions, two types of test were performed: (a) stress relaxation (using a step function shear strain); and (b) stress relaxation after cessation of steady shear flow

at sufficiently low shear rates, $\dot{\gamma}_0 < \dot{\gamma}_0{}^*$, where $\dot{\gamma}_0{}^*$ denotes the shear rate at which the viscosity function $\eta(\dot{\gamma})$ starts to deviate from the limiting value η_0, compare *Figure 3*. By means of (a), the shear relaxation modulus $G(t)$ is determined. It is the linear viscoelastic shear relaxation modulus, $G^\circ(t)$, if the height γ_0 of the step function shear strain is so small that the modulus is independent of γ_0. In the linear viscoelastic range, the material response to a step function shear rate ('stressing experiment') is the stress growth $p_{12}(t)$, from which we define a linear viscoelastic material function called here the 'stressing viscosity'*:

$$\eta^\circ(t) \overset{\text{def}}{=} p_{12}(t)/\dot{\gamma}_0. \quad (\dot{\gamma}_0 < \dot{\gamma}_0{}^*) \tag{4}$$

Stressing viscosity and relaxation modulus are related[14] by the equations

$$\frac{\mathrm{d}\eta^\circ(t)}{\mathrm{d}t} = G^\circ(t) \text{ and } \eta^\circ(t) = \int_0^t G^\circ(t)\,\mathrm{d}t \tag{5}$$

For the stress relaxation in test (b), a new time variable t' is introduced such that $t' = 0$ at the instant of cessation of flow. From the theory of linear viscoelasticity, the following relation between stressing viscosity and stress relaxation $p_{12}(t')$ after cessation of sufficiently long ($t \to \infty$) steady shear flow can be derived:

$$\eta^\circ(t)\Big|_{t=t'} = \frac{p_{12}(t'=0)}{\dot{\gamma}_0} - \frac{p_{12}(t')}{\dot{\gamma}_0} = \eta_0 - \frac{p_{12}(t')}{\dot{\gamma}_0} \tag{6}$$

This equation shows the symmetry between stress growth and stress relaxation after cessation of steady shear flow, test (b), provided that the deformation is in the linear viscoelastic range and the equilibrium shear stress is achieved before the shear deformation is stopped.

From equation 6, the reduced linear viscoelastic stressing viscosity may be defined as follows:

$$\eta^\circ(t)/\eta_0 = 1 - p_{12}(t')/p_{12}(t'=0) \tag{7}$$

This function describes the transient behaviour without the influence of the (slightly) different zero shear viscosity η_0 of the three samples.

In order to perform the relaxation test (a), the Weissenberg rheogoniometer was used with a proper modification[10] to impose a step shear strain rapidly (within 0.01 s). The measurements were made at 150°C only. *Figure 4* gives the functions $G^\circ(t)$ obtained. It follows from this plot that there are only small differences between the three samples. For short times t, the moduli are practically equal, whereas for longer times the differences increase. These differences are seen more clearly in *Table 12*. According to this result, material C relaxes more quickly than A, and A more quickly than B. However, the differences are very small, about ± 10 per cent or less.

---

* This notation was formulated by Giesekus[14]. Other authors, too, feel that $\eta^\circ(t)$ as a linear viscoelastic material function should have a separate name; e.g., Tschoegl[15] speaks of 'relaxance coefficient'. Several members of the Working Party do not agree with the term 'stressing viscosity' and propose 'transient viscosity' instead. The writer of this report feels, however, that 'transient' is too general, whereas 'stressing viscosity' has the advantage that it requires one to go back to the definition, i.e. equation 4.

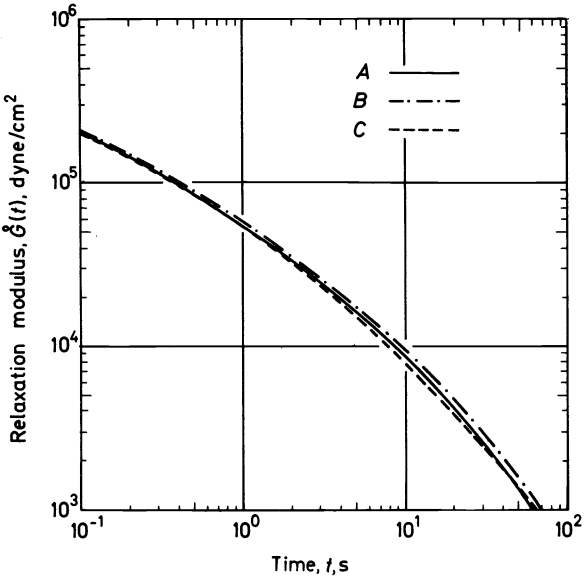

Figure 4. Shear relaxation modulus $G^{\circ}(t)$ from stress relaxation after step function shear strain. Temperature 150°C, from IV.

Table 12. Shear relaxation muduli $G^{\circ}(t)$; T = 150°C

	A	B	C
t = 0.1 s	2.0	2.04	1.97 × 10^5 dynes/cm^2
1 s	5.4	5.7	5.3 × 10^4 dynes/cm^2
10 s	8.6	9.6	7.8 × 10^3 dynes/cm^2

Participant II performed test (b) (stress relaxation after cessation of steady shear flow) at 130, 150 and 190°C. At all these temperatures, no distinct differences in the behaviour of the three samples could be detected. IV measured at 150°C only, with a somewhat extended time scale. For this temperature, the results* from II and IV are shown in *Figure* 5 as reduced stressing viscosity which was determined with the help of equation 7. Considering the scatter of the results†, we can conclude that the curves $\eta^{\circ}(t)$ from the two participants fall together, in general, and that they coincide sufficiently for the different samples A, B, C. The data of IV have a little less scatter, and they indicate that the reduced stressing viscosity for A and C seems to be exactly

* During these tests it is important to ensure that the stress level, from which the relaxation begins, is within the linear viscoelastic range.

† For these transient experiments, the apparatus has to be extremely stiff. Otherwise the strain in the specimen cannot instantaneously be made zero, due to the recovery of the torque measuring system; compare Figure 5 of ref. 10.

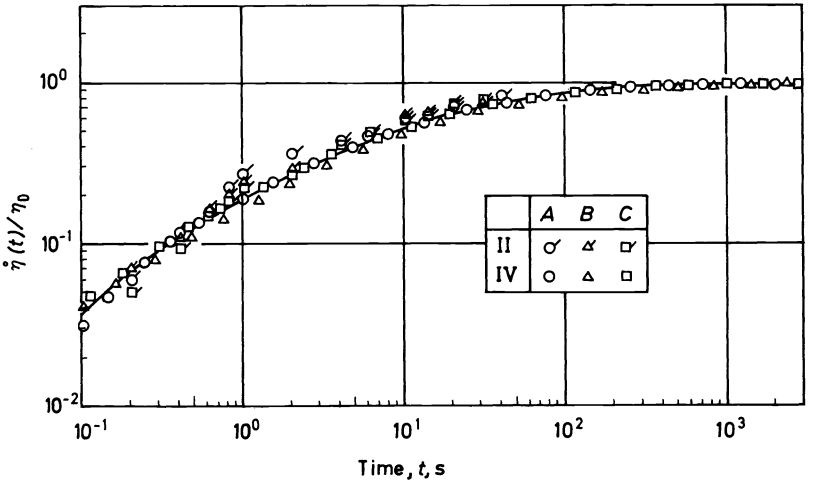

Figure 5. Reduced stressing viscosity $\eta^\circ(t)/\eta_0$ determined by stress relaxation after cessation of steady shear flow at $T = 150°C$.

the same whereas for sample B, $\eta^\circ(t)/\eta_0$ seems to increase more slowly at longer times of shear. To demonstrate this difference clearly, *Table 13* gives the times t' at which $\eta^\circ(t)|_{t=t'} = 0.50\,\eta_0$ and $0.90\,\eta_0$. The data from this table confirm the result already formulated.

Table 13. Relaxation times t' of test (b) at which the stressing viscosity $\eta(t)|_{t=t'}$ is equal to 50 per cent and 90 per cent of the equilibrium value η_0 (data from IV)

	A	B	C	
$t' = t(\eta = 0.50\,\eta_0)$	9	11.3	8.3	s
$t' = t(\eta = 0.90\,\eta_0)$	150	210	170	s

The advantage of test (b) lies in its more slowly relaxing stress signal for long experimental times when compared with test (a). Therefore, it is more convenient to calculate the shear modulus $G^\circ(t)$ for long times t from the slope $d\eta^\circ(t)/dt$ of the stressing viscosity according to equation 5. There is the additional advantage that, for short relaxation times, the coincidence of the two tests can be checked by comparing the calculated modulus with the directly measured one*.

The results of this procedure are given in *Table 14*. For the three times 0.1–1.0–10 s, the moduli determined by the two methods are sufficiently close for each material (about ten per cent difference). Secondly, the table shows that

* For a detailed discussion of such a comparison, including $G^\circ(t)$ calculated from the frequency-dependent functions $G'(\omega)$ and $G''(\omega)$, reference 10, Figure 8 should be consulted. Such a comparison confirms the validity of the linear viscoelastic treatment for the test conditions applied.

Table 14. Comparison of the linear viscoelastic shear relaxation modulus $G°(t)$, measured directly in the relaxation experiment [test (a)] and calculated from relaxation after steady shear flow [test (b)] by means of equation 5; data from IV

t, s	Type of test	A	B	C
0.1	(a)	200000	204000	197000 dynes/cm^2
	(b)	208000	197000	189000 dynes/cm^2
1.0	(a)	54000	57000	53000 dynes/cm^2
	(b)	50500	49500	52500 dynes/cm^2
10	(a)	8600	9600	7800 dynes/cm^2
	(b)	8600	8800	8100 dynes/cm^2
100	(a)	—	—	—
	(b)	520	650	465 dynes/cm^2
1000	(a)	—	—	—
	(b)	9.4	15	8.3 dynes/cm^2

test (b) allows one to determine moduli down to very small values of about 10 dynes/cm^2. From the comparison of the three samples, it follows that there are only minor differences with respect to $G°(t)$: in the whole range of time t, sample C has the smallest modulus. At short times, the three samples have practically the same modulus, whereas for longer times ($t > 10$ s) B has a larger modulus than A or C.

(C1.3) *Frequency-dependent linear viscoelastic material functions*

For the dynamic mechanical measurements, three different types of apparatus were used: the Weissenberg rheogoniometer by I (at 130 and 190°C, $0.04 \leqslant \omega \leqslant 80\,s^{-1}$); the Kepes Balance Rheometer[16] by II (at 150°C, $0.008 \leqslant \omega \leqslant 80\,s^{-1}$); and the TNO Couette type instrument[17] by IV (at 150°C, $0.01 \leqslant \omega \leqslant 100\,s^{-1}$). I tested stabilized material, in addition, and found remarkable differences between the 'as received' and the 'stabilized' specimens of the same sample A, B or C at 190°C. Therefore, the results at this temperature will not be discussed here*.

At 130°C, I found within the scatter of the results the same linear viscoelastic material functions for the three samples, i.e. the same storage and loss modulus as functions of the circular frequency $\omega = 2\pi\nu$. These functions have the same forms at 130 and 150°C; it is therefore sufficient to give data for one of these temperatures only. *Table 15* presents three different sets of data obtained at 150°C by three operators using two different instruments. The data obtained by different operators with the same instrument are, in general, in excellent agreement. The agreement between the data obtained with different instruments, is less than perfect but is still reasonable. It is quite obvious from the results reported in the table that no significant differences exist between the three samples as far as linear viscoelastic behaviour is concerned. At low frequencies, II finds systematically lower values for G' and G'' in the case of sample A compared with samples B and C. Lower values for sample A in the range of lower frequencies are also found by IVa, but contrary to the findings of II, the difference between the values of G' for samples B and C is found by IVa

* Compare also section A7 'Thermal stability of the melts'.

to be of the same order of magnitude as the difference between A and B. All sets of data agree with respect to the effect of increasing frequency which tends to diminish the observed differences between the samples.

Table 15. Storage modulus G' and loss modulus G'' at 150°C in dynes/cm^2

1. G'

ω [s^{-1}]	Sample	II (Dr Aßsioma)	IVa (Dr Zosel)	IVb (Dr Münstedt)
0.01	A	1.01×10^3	1.05×10^3	1.12×10^3
	B	1.46×10^3	1.40×10^3	1.16×10^3
	C	1.53×10^3	1.09×10^3	8.5×10^2
0.1	A	1.39×10^4	1.20×10^4	1.26×10^4
	B	1.81×10^4	1.40×10^4	1.30×10^4
	C	1.70×10^4	1.27×10^4	1.18×10^4
1	A	8.10×10^4	7.0×10^4	7.0×10^4
	B	8.70×10^4	7.3×10^4	7.3×10^4
	C	8.60×10^4	7.35×10^4	7.0×10^4
10	A	2.70×10^5	2.6×10^5	2.45×10^5
	B	2.85×10^5	2.8×10^5	2.49×10^5
	C	2.80×10^5	2.6×10^5	2.60×10^5
100	A	6.80×10^5*	7.0×10^5	
	B	7.20×10^5	7.1×10^5	
	C	7.00×10^5	7.1×10^5	

2. G''

0.01	A	4.76×10^3	4.2×10^3	4.7×10^3
	B	5.50×10^3	4.5×10^3	4.5×10^3
	C	5.70×10^3	4.55×10^3	4.25×10^3
0.1	A	2.65×10^4	2.24×10^4	2.25×10^4
	B	2.90×10^4	2.41×10^4	2.38×10^4
	C	2.83×10^4	2.38×10^4	2.30×10^4
1	A	8.90×10^4	8.15×10^4	7.7×10^4
	B	9.00×10^4	8.40×10^4	8.20×10^4
	C	8.80×10^4	8.50×10^4	8.30×10^4
10	A	1.98×10^5	2.10×10^5	1.95×10^5
	B	2.05×10^5	2.20×10^5	2.0×10^5
	C	2.07×10^5	2.20×10^5	1.92×10^5
100	A	3.70×10^5*	4.80×10^5	
	B	3.70×10^5	4.65×10^5	
	C	3.70×10^5	4.70×10^5	

* Extrapolated.

The differences between the data obtained with different instruments also seem to be frequency-dependent: with increasing frequency, the difference between G' values decreases. The difference between the G'' values appears to change sign for frequencies higher than 10 s^{-1}. Taking account of the limited

accuracy of the oscillatory measurements, the general behaviour of G' and G'' as a function of frequency (*Figure 6*) is in good agreement with the results of the relaxation measurements (see also Figure 8 of ref. 10).

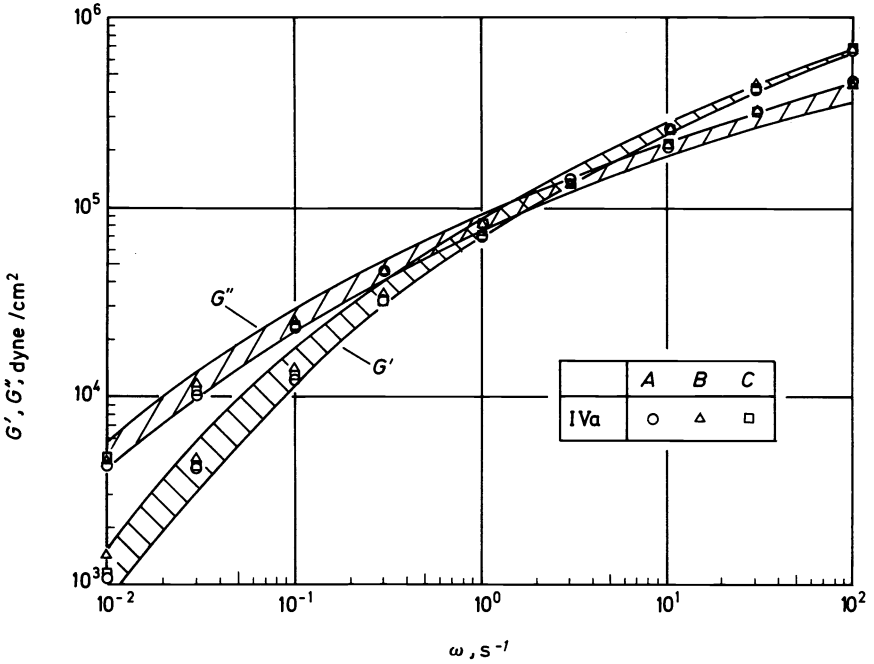

Figure 6. Frequency dependent storage modulus $G'(\omega)$ and loss modulus $G''(\omega)$ at $T = 150°C$. The points denote the results of IVa (Dr Zosel); the hatched areas represent the range of data given in *Table 15*.

(C1.4) *Conclusions of section C1*

Generally speaking, there are practically (i.e. within ten per cent) no differences in the linear viscoelastic behaviour of the three samples. The zero shear viscosity η_0 at different temperatures coincides within ± 10 per cent for all the participants and samples. These differences between η_0 of A, B and C are still further reduced (absolute value of the maximum difference ten per cent), when measured by the same participant.

In linear viscoelastic behaviour at 150°C, the time-dependent material functions relaxation modulus and stressing viscosity are equal (also within ten per cent); only at $t > 100$ s sample B seems to have a slower relaxation. The oscillatory results, G' and G'', are equal for the three samples at frequencies $\omega > 1\ s^{-1}$. At $\omega < 0.1\ s^{-1}$, different participants obtain differences in ordering A, B, C with respect to G' and G''. These discrepancies reflect open problems in obtaining accurate data with the instruments and conditions used.

The temperature dependence of η_0 (expressed by the activation constant E_0) is the same for A, B and C. If the molten samples can be treated as thermorheologically simple materials[18], it follows from the time–temperature

superposition principle[19] that the validity of the conclusion concerning the identical linear viscoelastic behaviour for 150°C can be extended to other temperatures for the molten state of the samples.

(C2) The viscosity function

The viscosity function $\eta(\dot{\gamma})$, commonly used to represent the non-Newtonian behaviour of polymer melts, is determined by measurement: at low rates of shear by means of rotational viscometers (compare the results from cone-and-plate instruments, *Figure 3*) and at higher shear rates by means of capillary viscometers using two types of corrections: (a) the Weissenberg correction[20] yields the true shear rate at the die wall for non-Newtonian liquids independent of the velocity distribution within the die; (b) the Bagley correction[21] provides the true pressure gradient from which the true shear stress at the die wall is calculated. In practice, the Weissenberg correction is a matter of calculation, using only the output rate as a function of wall shear stress. The Bagley correction, however, requires the measurement of output rate as a function of extrusion pressure for different values of L/R (die length/die radius).

Two comments should be made. (1) Measurements with the rotational system indicate a time-dependent shear stress $p_{12}(t)$ at constant shear rate $\dot{\gamma}_0$. At low shear rates, the stressing viscosity $\eta^+(t)$ is measured with the equilibrium value η_0 which is used for the representation here. At higher shear rates, however, the stressing viscosity $\eta(t)$ shows a maximum (compare Figure 15 of ref. 10). This time dependence will be discussed in section C4; here, data for the rotational system are considered for low shear rates only. (2) The capillary viscometer connects one shear rate with only one pressure or (at different die lengths) with pressure differences. Therefore, this instrument does not, in general, give any information concerning the time dependence of flow behaviour (exception: dependence of extrudate swell on die length, see section C3).

In addition to the rotational rheometers described in section C1, the following capillary viscometers were used: The Monsanto–Instron Capillary Extrusion Rheometer[22] with 90° die entrance angle and 1.59 mm die diameter by Ib, and a gas-driven capillary viscometer[23] with 180° die entrance angle ('flat' dies) and 1.200 mm die diameter by IVb. In both instruments, dies of different lengths were used in order to make the Bagley correction.

The results for lower shear rates were shown already in *Figure 3* for the temperature range 112–190°C. The measurements at higher shear rates with the capillary viscometer were performed at 150 and 190°C. All the viscosity data at these two temperatures are given in *Figure 7*. The data cover the remarkably wide range of shear rates from 10^{-4} to $10^{+3}\ s^{-1}$. At first sight, the results for the three samples measured by five different instruments coincide very well at 150°C, but there are clear differences at 190°C, not for the different samples but for the different participants, i.e. for different test methods. This fact again demonstrates the importance of thermal stability if reliable data are to be discussed. For any one participant, the three samples again show practically identical curves, for 190°C as well as for 150°C.

For a discussion in more detail, the results at 150°C were interpolated graphically and the viscosity data tabulated for fixed decades of shear rate (*Table 16*). At low shear rates, the coincidence of the data within ± 10 per cent is again evident. At 0.1 and $1\ s^{-1}$, a similar coincidence is evident, even when the capillary results IVb are included; the coincidence at $1\ s^{-1}$ is even better. At

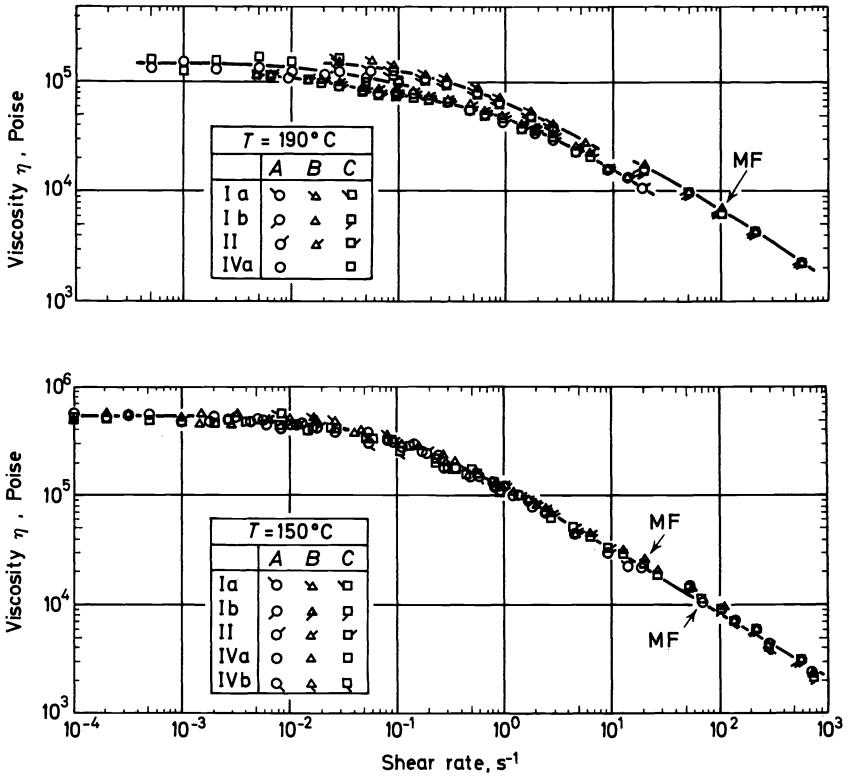

Figure 7. Viscosity functions for samples A, B, C at 150°C and 190°C. Ia, IVa: Weissenberg rheogoniometer (Ia measures at 130°C and shifts the data); II: Kepes rotational rheometer (cone-and-plate); Ib, IVb: capillary viscometers. MF denotes the onset of melt fracture.

higher shear rates, the two capillary instruments give good agreement (difference about ten per cent). Only at $10\,s^{-1}$ is there a more pronounced difference between the rotational (II) and the two sets of capillary data. However, this may be due to the pronounced time dependence of viscous flow at this relatively high shear rate (see also section C4).

Comparing the three samples for each participant separately, the ten per cent difference at the lowest shear rates denotes the largest difference between the viscosity data measured. At higher shear rates, the magnitude of this difference is reduced below ten per cent to such an extent that the viscosity functions of the three samples at 150°C can be assumed to be identical. The identity of the viscous behaviour was one criterion for the selection of the three samples for this programme. The present result confirms that this criterion is fulfilled. The final conclusion has to be that neither the linear viscoelastic nor the purely viscous behaviour of the melts reflects the differences which are found in the processing behaviour and in the end-use properties described in section B.

Table 16. Shear viscosity $\eta(\dot{\gamma})$ at $T = 150°C$. Obtained by graphical interpolation to the fixed shear rates $\dot{\gamma}$ indicated. Ia uses a shear rate–temperature shift method in order to determine the viscosity function at 150°C from data measured at 130°C. For the other test methods, see the legend to *Figure 7.*

$\dot{\gamma}$, s^{-1}	From	A	B	C	
0.0001	IVa	5.5	5.5	5.0	10^5 Poise
0.001	Ia	4.2	5.2	—	10^5 Poise
	II	4.7	4.8	4.9	10^5 Poise
	IVa	5.5	5.5	5.0	10^5 Poise
0.01	Ia	4.2	5.2	4.95	10^5 Poise
	II	4.4	4.5	4.7	10^5 Poise
	IVa	4.4	4.85	4.35	10^5 Poise
0.1	Ia	3.17	3.4	3.0	10^5 Poise
	II	3.1	3.2	3.2	10^5 Poise
	IVa	2.90	2.90	2.82	10^5 Poise
	IVb	2.85	3.0	3.0	10^5 Poise
1.0	Ia	1.23	1.23	1.22	10^5 Poise
	II	1.1	1.18	1.18	10^5 Poise
	IVb	1.18	1.21	1.20	10^5 Poise
10	Ib	4.0	3.95	3.88	10^4 Poise
	II	2.9	3.2	3.1	10^4 Poise
	IVb	3.6	3.65	3.41	10^4 Poise
100	Ib	10.3	10.3	9.6	10^3 Poise
	IVb	8.8	8.8	8.8	10^3 Poise
1000	Ib	2.2	2.2	2.11	10^3 Poise
	IVb	2.0	1.93	1.92	10^3 Poise

(C3) Elastic effects in extrusion flow

In contrast to the former results of sections C1 and C2, the three samples show differences in the elastic effects during melt extrusion. In the following sections, short descriptions of the test procedures are given in those cases for which new or improved measuring techniques were used.

(C3.1) *End correction in capillary flow*

The end correction e in capillary flow according to Bagley[21, 24] is related to the true shear stress p_{12} at the die wall, the extrusion pressure p, and the derivative $\partial p/\partial z$, as follows:

$$p_{12} = \frac{R}{2} \cdot \frac{\partial p}{\partial z} = \frac{R}{2} \cdot \frac{p}{L + eR} = \frac{1}{2} \frac{p}{e + L/R} \tag{8}$$

where R denotes radius, L is the length of a capillary die, and z, the coordinate in the direction of the die axis.

This equation involves the assumption that the pressure gradient $\partial p/\partial z$ is constant within the die. In that case the extrusion pressure should vary

linearly with L/R for constant shear stress p_{12} and, therefore, also for constant 'apparent shear rate' $D = 4q/\pi R^3$ (q is the volume output rate). In such a graph of $p(L/R)$ for D = constant (Bagley plot), e is found by extrapolation of the straight lines to $p = 0$: $e \stackrel{\text{def}}{=} -L/R$ for $p \to 0$. Experimentally, the output rate q is determined as a function of pressure in a capillary viscometer using several dies of different L/R ratios. From these functions, the Bagley straight lines are plotted which yield $e(D)$ or $e(p_{12})$.

Two laboratories participated in these tests: I used a Monsanto Capillary Extrusion Rheometer[22], cylinder diameter 9.53 mm, with six dies of 1.59 mm diameter, L/R ratios between 0 and 40, all of tapered entrance angle (90°). IV used a gas-driven capillary viscometer[23], cylinder diameter 15.3 mm with two sets of dies, IVa five dies of 1.200 mm diameter, L/R between 1.5 and 30, IVb 13 dies of 3.000 mm diameter, L/R between 0.4 and 70. All dies IVa or IVb were 'flat' (180° entrance angle). It should be noted that the evaluation of the measured data was different. I used a computer with a linear correlation programme; in IVa, the best straight line was drawn through all the points for D = constant in the Bagley plot, and in IVb only the points of the largest L/R ratios were used to determine these straight lines*.

The end corrections at 150°C are plotted in *Figure 8* as a function of the apparent shear rate D. e increases with D, but there are remarkable differences between the results from the different test methods. Comparing the three samples, the three methods yield the same result. Sample A has a distinctly higher end correction than has B or C. Concerning B and C, two ranges exist: (1) flow without melt fracture; B and C show (except for very low shear rates) nearly the same end correction; (2) flow with melt fracture; I reports again the same result as in (1), while IVa finds e values for B which are equal to those for A and higher than those for C.

For a more detailed discussion, the end corrections e(A) and e(B) for samples A and B are related to the end correction e(C) of sample C in *Table 17*. This table confirms the results already stated. It is interesting to note that the largest deviations from the ratio 1 are found at the low apparent shear rates $D = 0.1$ and $1\ s^{-1}$; this shows that differences in the elastic properties of the three samples—if the end correction is a true reflection of the elastic properties—appear more clearly at lower shear rates.

The results at 190°C are not presented here. They give the same result found by I for 150°C as far as the differences in e for A, B and C are concerned.

(C3.2) *Separation of end correction e into elastic and geometric portions*

In order to divide the energy associated with the end correction into different additive contributions, a test method[12, 23] is used which depends on the assumption that in capillary flow the total energy input is utilized in the following three* ways:

* With dies of 3.00 mm diameter (IVb), it turned out that at higher shear rates the pressure values for short dies are lower and do not fall exactly on the straight line drawn through the points for the longer dies, e.g. in the Bagley plot of sample A for $D = 10\ s^{-1}$, all points for $L/R \leqslant 8$ are lower than the straight line defined by the points for $L/R > 12$. The deviations are small and can be detected only if the viscometer is equipped with high precision manometers. It should be pointed out that similar deviations were observed with other polymer melts also[25].

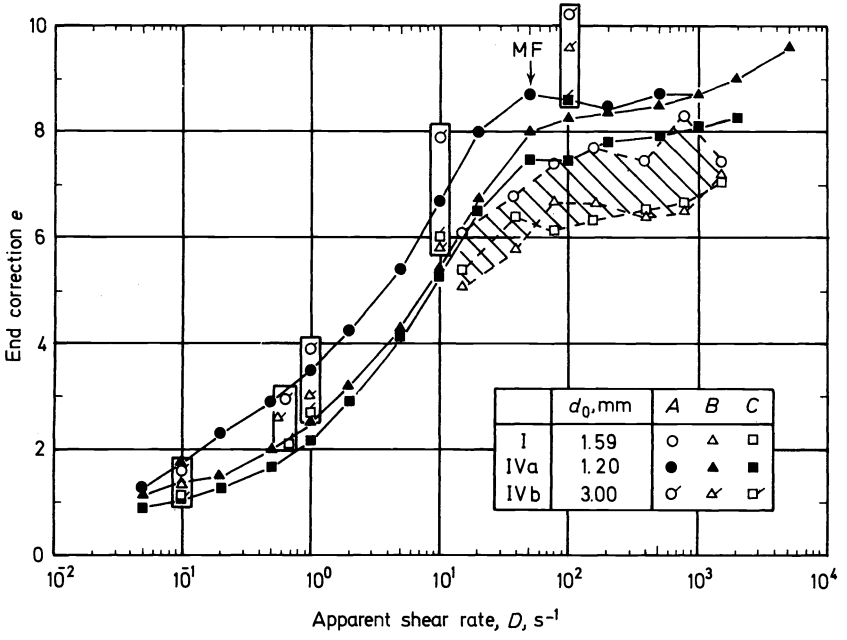

Figure 8. End correction e as a function of apparent shear rate at $T = 150°C$ for two different types of capillary rheometers; IV used two sets of capillaries with different L/R ranges (see text). The arrow MF denotes the onset of melt fracture.

Table 17. Ratios of end corrections e of samples A or B related to sample C, $T = 150°C$.

D, s^{-1}	Ref.	e(A)/e(C)	e(B)/e(C)
0.1	IV a	1.67	1.29
	IV b	1.45	1.18
1	IV a	1.63	1.16
	IV b	1.44	1.11
10	I	1.12*	0.93*
	IV a	1.28	1.04
	IV b	1.32	0.97
100	I	1.16	1.01
	IV a	1.15	1.11
	IV b	1.19	1.12
1000	I	1.19	1.03
	IV a	1.07	1.07

* Extrapolated.

I—energy dissipation (viscous flow) within the die;
II—generation of elastic energy in the streaming melt, causing for instance extrudate swell;
III—energy dissipation in the inlet region in front of the die due to secondary flow, converging flow, and elongational deformation of the streaming melt.

The separation into the three energy portions also involves an assumption that the formation of the secondary flow régime at the die entrance (and, correspondingly, the build-up of the entrance pressure loss) does not occur instantaneously, but needs time for a complete development.

The separation of the extrusion pressure p (denoting total input of energy density) into the three portions I, II and III is performed in the following way. After heating up the polymer material in the viscometer barrel of *Figure* 9(a), the die is shut and the pressure is applied to the viscometer. Five minutes later, the die is opened and the output rate (mass rate m) is measured as a function of time. During this test, the gas pressure on top of the polymer melt is kept constant. A mass rate/time function is obtained [see *Figure* 9(b)] which shows a maximum m_0 and a decrease to a minimum $\bar{m}$. It can be assumed that at m_0 there is no pressure loss at the die entrance yet, whereas at $\bar{m}$ the inlet region is developed completely. From m_0 and $\bar{m}$ two apparent shear rates, D_0 and $\bar{D}$, are calculated. Accordingly, two Bagley plots are obtained, for D_0 = constant and for $\bar{D}$ = constant, *Figure* 9(c). The Bagley plots yield two end corrections, e_0 and $\bar{e}$. e_0 is the elastic portion; the difference $(\bar{e} - e_0)$ is the geometric portion of the total end correction $\bar{e}$. $\bar{e}$ corresponds to the end correction e of the previous section C3.1†.

The measurements were performed at 150°C with the set of dies IVa (section C3.1). For $D < 5\,s^{-1}$, no maximum in the $m(t)$ curve is found, indicating that no pressure loss in the die entrance region can be detected; thus, for $D < 5\,s^{-1}$, the relation $\bar{e} = e_0$ holds. For $D > 2000\,s^{-1}$, the height of the maximum m_0 cannot be measured exactly. Therefore, $e_0(D_0)$ can be obtained for the range $5\,s^{-1} < D_0 < 2000\,s^{-1}$ only. A very important experimental observation must be added: in the whole range D_0 indicated, no melt fracture occurs; in other words, in all cases the extrudate is smooth for all values of D_0 as long as the extrudate is cut-off within a short extrusion period corresponding to the maximum of the curves *Figure* 9(b). If the output rate is high enough, the onset of melt fracture starts to occur in the decreasing region of the $m(t)$-curve‡.

---

* According to Malkin *et al.*[26], a fourth source of energy consumption should be added which corresponds to the work necessary for the 'structure breakdown' of the melt during flow, compare also section C4.

† From a more physical point of view, consideration of the ordinate intercepts seems to be preferable[27]. For D_0 = constant, $p(L/R \to 0)$ yields the energy density portion II (previously denoted by p_0); for $\bar{D}$ = constant, the ordinate intercept yields the sum II+III, as is indicated in *Figure* 9(c). The (maximum) elastic energy density, reflected by II, is not constant within the die but decreases remarkably with die length increase, as follows from the extrudate swell measurements (compare the following section C3.3).

‡ This behaviour was demonstrated previously[28] for high density polyethylene with the well-known sudden increase in output rate at the onset of melt fracture.

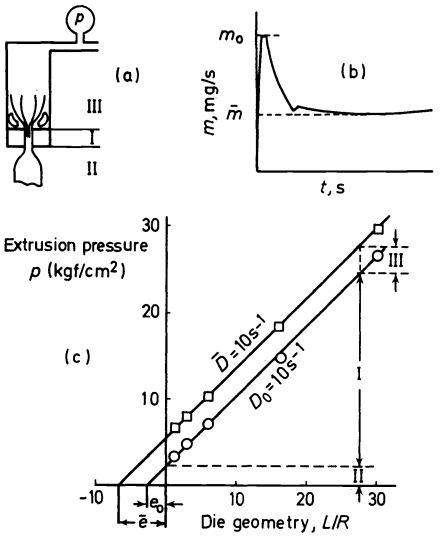

Figure 9. Energy consumption in extrusion. and separation of end correction into geometric and elastic portions. (a) Schematic representation of the three energy densities I–II–III, which add up to the total extrusion pressure p; (b) Time-dependent output rate (schematic), when a die shut-off device is opened at $t = 0$; (c) Bagley plots for the two numerically equal apparent shear rates $D_0 = \bar{D} = 10\,s^{-1}$. D_0 corresponds to output rate m_0 (assumption: no pressure loss III in the inlet region), and $\bar{D}$ corresponds to $\bar{m}$ (assumption: completely developed inlet region in front of the die entrance). The data plotted in (c) were measured with sample A at 150°C, and die diameter $d_0 = 2R = 1.200$ mm: results from IV.

Figure 10 gives the $e_0(D_0)$ relation for the three samples. In the whole D_0 shear rate range, sample A has the highest, and sample C the lowest, e_0 values. Sample B, and this is a remarkable result, is similar to sample C at low shear rates, but increases more rapidly with D_0 so that, for higher shear rates, B gives the same e_0 as sample A. There is even an indication (at $D_0 = 10^3\,s^{-1}$) that

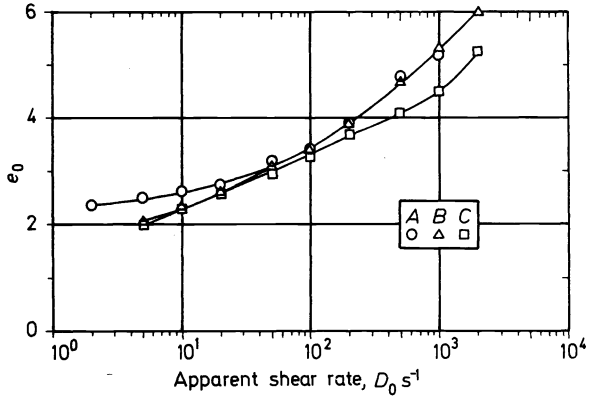

Figure 10. Elastic portion e_0 of the total end correction in capillary flow as a function of the apparent shear rate D_0. Die diameter $d_0 = 1.200$ mm, $T = 150$°C; results from IV.

within a certain shear rate range sample B has a slightly higher e_0 than A.

Comparing the end correction e of *Figure 8* (corresponding to $\bar{e}$ in our present notation) and e_0 of *Figure 10*, it turns out that the comparison of samples A, B and C leads to the same general statement: at low shear rates, B is very similar to C, whereas at high shear rates, B is similar to A. A shows the highest, and C the lowest, $\bar{e}$ and e_0 curves in the shear rate range investigated. However, there are quantitative differences: in the shear rate range 50–100 s^{-1}, the e_0 values fall close together for the three samples, which is not the case for $\bar{e}$. In the representation of *Figure 8*, the comment should be made that in the range $\bar{D}$ = 20–50 s^{-1}, melt fracture starts to occur (compare section C3.4) which is never the case throughout the D_0 range of *Figure 10*. In conclusion, if e_0 represents the elastic deformation connected with viscous flow in capillary extrusion, sample A is more elastic than B or C at low shear rates, and C is less elastic than A or B at high shear rates. The same conclusion follows for the total end correction $\bar{e}$ (= e of *Figure 8*) if this quantity is considered to represent the elastic deformation connected with capillary flow.

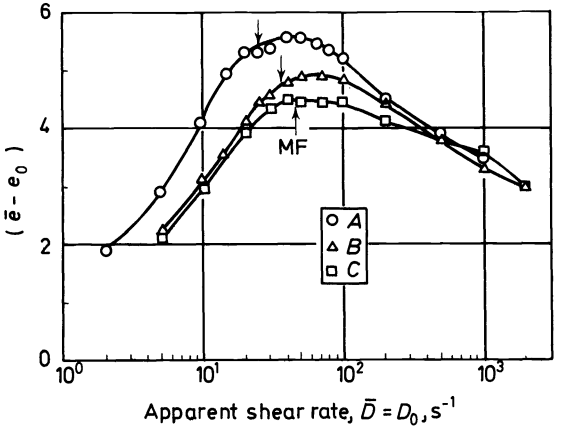

Figure 11. Geometric portion $(\bar{e} - e_0)$ of the total end correction in capillary flow as a function of the apparent shear rate $\bar{D} = D_0$. The quantity recorded reflects the energy consumption in front of the die at least for $D < D_{crit}$ (D_{crit} denotes critical apparent shear rate for the onset of melt fracture marked by MF). Die diameter d_0 = 1.200 mm, T = 150 C; results from IV.

An interesting conclusion can be drawn from a consideration of the geometric portion $(\bar{e} - e_0)$ of the end correction. The shear stress p_{12} (which has not very different values for A, B and C) and $\bar{e} - e_0$ determine the value p(III) (denoted by III in *Figure 9*) of the inlet region pressure loss according to the equation $p(\text{III}) = (\bar{e} - e_0)\, pR/\Delta L = 2(\bar{e} - e_0)\, p_{12}$, which follows from *Figure 9* and equation 8. *Figure 11* shows that $(\bar{e} - e_0)$ is significantly greater for sample A than for B or C, as long as the shear rate D is lower than the critical shear rate $D_{crit} \approx$ 20–50 s^{-1} for the onset of melt fracture (compare section C3.4). For $D > D_{crit}$, the significance of the figure is not clear because in this case the quantities subtracted, $\bar{e}$ and e_0, are related to different flow situations (stable for e_0, unstable for $\bar{e}$). The unquestionable conclusion which can be drawn from *Figure 11* is that for stable flow the pressure loss in the entrance

region, in other words the energy consumption in front of the die entrance, is significantly larger for sample A than for the samples B or C.

(C3.3) *Extrudate swell*

In the capillary extrusion of the polymer melts, the extrudate diameter is larger than the die diameter. This effect is called extrudate swell* and in many publications is attributed to the elastic recovery of the melt emerging from the die, e.g. in refs. 29, 30, 31. Participant IV used the gas-driven capillary viscometer described in section C3.1 with the die set IVb (die diameter $d_0 = 3.00$ mm). All dies were 'flat' (180° entrance angle). The extrusion pressure was always adjusted for the different dies such that the output rate corresponded within ± 1 per cent to a pre-selected constant apparent shear rate $\bar{D}$. In order to obtain results of little scatter, the following procedure[27] was used: after the steady output rate $\bar{m}$ was achieved [compare *Figure 9*(b)], short cut-offs of 15–20 mm length were taken. These cut-offs were re-melted in a specially selected silicone oil for a period of 15 min at 150°C in order to obtain the equilibrium swell.

The extrudate swell ratio β at melt temperature T is calculated from the extrudate diameter d measured at room temperature by the following equation[32]

$$\beta = [v(T)/v(20)]^{\frac{1}{3}} \times d/d_0 \tag{9}$$

(T in °C; $v(T)$ and $v(20)$ denote specific volume at T and at room temperature; for $T = 150$°C, IV used the constant $[v(T)/v(20)]^{\frac{1}{3}} = 1.0565$).

Participant V applied a similar procedure to obtain extrudate swell data (gas-driven capillary viscometer of different type, $d_0 = 1.440$ mm, cylinder diameter 15.7 mm); the cut-offs were collected as by IV and annealed in silicone oil at 115°C for 90 min†.

The functions $\beta(L/R)$ obtained by IV are given in *Figure 12* for constant apparent shear rate $D(\pm 1$ per cent) and in *Figure 13* for constant true shear stress p_{12}. From these figures, a tremendous decrease of β with increasing L/R is evident, especially for short dies. It is remarkable that only at the lowest shear rate $D = 0.1\ s^{-1}$ is the equilibrium swell $\beta(L/R \to \infty)$ for the sufficiently long (infinitely' long) die obtained within the die lengths used. Comparing the three samples, β for A is higher than β for B or C at the same shear rates. However, at $D = 10\ s^{-1}$, the result is different and more complex: for short dies, sample B has the highest extrudate swell, whereas for long dies

* In the engineering literature, the term 'die swell' is used which should be avoided because of its deceptive character.

† There is an important difference in the procedures of IV and V in so far as IV referred the die swell data to a constant apparent shear rate (i.e. constant output rate) or a constant true shear stress (i.e. pressure gradient within the die), whereas V referred the results to a constant apparent shear stress. Because of the different end corrections of the three samples (section C3.1), the β values and their dependence on die length, $\beta(L/R)$, cannot be compared directly. However, the procedure of *V* is often applied in the plastics industry. It is a matter of discussion whether β values for different samples should be compared at constant shear rate or constant (true) shear stress. In the case of A, B and C, this problem is unimportant in so far as the viscosity functions, in the shear rate range used here, are practically the same (difference less than ten per cent, compare *Table 16*).

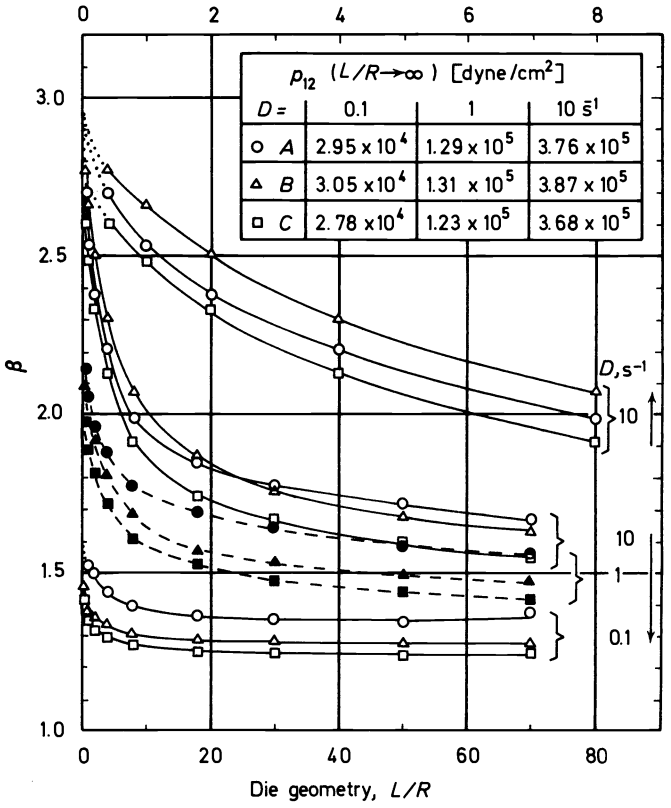

Figure 12. Extrudate swell ratio $\beta(L/R)$ at different apparent shear rates D. For $D = 10\,s^{-1}$, a second, extended L/R axis is used (upper curves). The table gives the true shear stress at the die wall for the different D values. $T = 150°C$, $d_0 = 3.00$ mm, results from IV. Notice that the shear stresses given in the table do not fit exactly the viscous data IVb of *Table 16*. In *Table 16*, IVb means results from the gas driven capillary viscometer of IV using dies of 1.200 mm diameter.

the highest swell is that of sample A. Correspondingly, there is a crossover of the functions $\beta(L/R)$ for A and B at $D = 10\,s^{-1}$. This is a very important finding which demonstrates that not only the absolute extrudate swell values but also the relative values for the three samples depend not on shear rate alone but also on additional parameters such as the average flow time or average total deformation. The measurements at the constant shear stress $p_{12} = 10^5$ dynes/cm^2 do not give results substantially different from those already found at $D = 0.1$ and $1\,s^{-1}$*. For a more detailed discussion, *Table 18* gives the β data of IV for $L/R = 0$, 8, 50 and ∞. For $L/R \to 0$ and ∞, the data reported are extrapolated; in the last case ($L/R \to \infty$), a method similar to the method 'X' of Tobolsky and Murakami[33] has previously[27] been found to be appropriate.

* Because of the different apparent shear rates D for p_{12} = constant in *Figure 13*, it should be noted that the average residence time (flow time in the capillary) of the samples is different. For this residence time, Bagley *et al.*[32] give the relation $t_a = 4\,L/RD$.

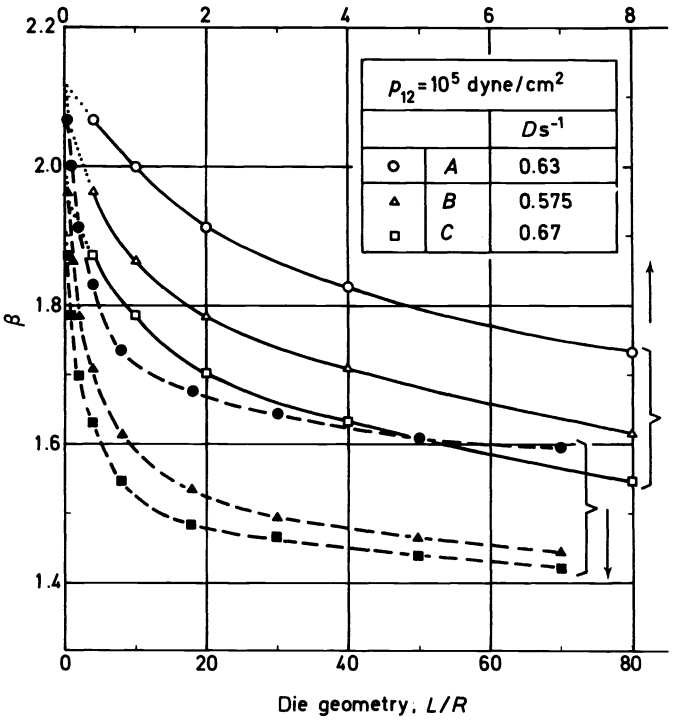

Figure 13. Extrudate swell ratio $\beta(L/R)$ at the true constant shear stress $p_{12} = 10^5$ dynes/cm^2. The table denotes the corresponding apparent shear rates D. $T = 150°C$, $d_0 = 3.00$ mm; results from IV.

A comparison of the three samples is easily made by using the last two columns of the table relating β(A) and β(B) to β(C). For $L/R = 0$, these columns show practically the same numbers, whereas for $L/R \neq 0$ differences exist which depend on the values of β(A), β(B) and β(C). From the table, it follows that, for $L/R \to 0$, $\beta(A) \approx \beta(B)$, and for $L/R \to \infty$, $\beta(B) \approx \beta(C)$, except at $D = 10\,s^{-1}$ where approximately the relation $\beta(A) \approx \beta(B)$ holds independent of L/R (note the crossover in the graph *Figure 12* for $D = 10\,s^{-1}$).

Table 19 gives the results obtained by V using two dies of different L/R ratios. As already pointed out, the absolute numbers of the two *Tables 18* and *19* cannot be compared. With the lower part of *Table 19* (for $L/R = 28$), there is a qualitative agreement with *Table 18* in so far as the two columns on the right give the same order A, B, C for decreasing β at low shear stresses or shear rates, and the order B, A, C for higher stresses or shear rates. The upper part of *Table 19* does not agree with the results of *Table 18*. In this case of a relatively short die, the difference between the apparent and the true shear stress becomes vital. Because of the larger end correction e of sample A at low shear rate or, correspondingly, at the low shear stresses of the upper part of *Table 19*, the true shear stress for A is lower than for B or C for the same appa-

Table 18. Extrudate swell ratio β; $T = 150°C$, $d_0 = 3.00$ mm, results from IV

D, s^{-1}	L/R	β			$\frac{\beta(A)}{\beta(C)} - 1$, %	$\frac{\beta(B)}{\beta(C)} - 1$, %
		A	B	C		
0.1	0	1.58	1.59	1.49	6.0	6.7
	8	1.39	1.31	1.27	9.6	2.9
	50	1.34	1.28	1.24	8.1	2.9
	∞	1.34	1.26	1.24	7.8	1.2
1	0	2.25	2.23	2.06	9.2	8.3
	8	1.78	1.69	1.61	10.6	4.9
	50	1.59	1.49	1.44	10.3	3.6
	∞	1.52	1.44	1.39	9.4	3.6
10	0	2.95	2.95	2.78	6.1	6.1
	8	1.99	2.07	1.92	4.1	8.2
	50	1.72	1.68	1.59	7.8	5.4
	∞	1.56	1.57	1.49	5.1	5.7
$P_{12} = 10^5$ dyn/cm²	0	2.12	2.10	1.98	7.1	6.1
	8	1.73	1.61	1.55	12.2	4.5
	50	1.61	1.47	1.44	11.7	1.9
	∞	1.58	1.40	1.39	14.1	1.1

rent shear stress, thus permitting no reasonable comparison to be made for the different conditions in measuring β*.

Table 19. Extrudate swell ratio β; $T = 150°C$, $d_0 = 1.44$ mm, results from V.

Extrusion pressure, p [kgf/cm²]	App. shear stress $p_{12,a} = pR/2L$ [10^5 dyn/cm²]	β (average)			$\frac{\beta(A)}{\beta(C)} - 1$ [%]	$\frac{\beta(B)}{\beta(C)} - 1$ [%]
		A	B	C		
(1) Short die, $L/R = 6.8$						
5	0.35	1.79	1.81	1.67	7	8
10	0.71	1.95	2.01	1.83	6.5	10
20	0.141	2.03	2.18	1.93	5	13
30	0.212	2.26	2.19	2.16	5	1
50	0.353	2.19(?)	2.39	2.33	−6	2.5
(2) Long die, $L/R = 28$						
5	0.88	1.47	1.35	1.26	17	7
10	1.77	1.58	1.51	1.42	11	6
20	3.53	1.62	1.57	1.48	9	6
30	5.30	1.61	1.63	1.54	4.5	6
50	8.83	1.72	1.68	1.58	9	6
80	14.13	1.67	1.82	1.68	−1	8
120	21.2	1.74	1.92	1.71	2	12

* This is also the reason that extrudate swell measurements following the melt indexer practice (as performed, e.g. by V) are omitted here.

The results of the extrudate swell measurements can be summarized as follows. Reproducibility of the results is remarkably good if some essentials of the measuring technique are fulfilled. The swell ratio β is a function of shear rate or, correspondingly, of shear stress, and β is a distinct function of L/R, as is already known from the literature. At 150°C, sample C has the smallest β under all conditions applied. However, for A and B the comparison depends on the shear conditions: $\beta(A) > \beta(B)$ for lower shear rates or shear stress. For high shear rates, $\beta(A) < \beta(B)$ for short dies, but $\beta(A) > \beta(B)$ for long dies.

(C3.4) *Melt fracture*

Melt fracture means the occurrence of surface irregularities of the melt emerging from extrusion equipment such as a capillary viscometer. This effect is often described in the literature and was described in detail by Tordella[34]. Melt fracture starts to occur at a critical apparent shear rate D_{crit}, and usually the relation between the apparent shear rate and the extrusion pressure $\log D = f(\log p)$ is marked by a break at D_{crit}. Participant I used this change of slope in order to determine D_{crit} for experiments performed at 190°C. At 150°C, participants I and IV used visual inspection of the emerging melt, whereas VI measured the frequency of entrance flow irregularities by optical observation (glass windows mounted in the barrel). When the capillary die is replaced by a slit die, VI reports that no melt fracture occurs in slit extrusion for the apparent shear rate range applied ($D < 40\,s^{-1}$)*.

Table 20. Critical apparent shear rate, D_{crit}, for the onset of melt fracture

	d_0, mm	L/R	α[°]	T[°C]	A	B	C
I	1.59	0–120	90	190	150–225	95–120	110–145
	1.59	0–120	90	150	15–38	15	15
IV	3.00	8	180	150	23	32	38
	3.00	50	180	150	29	38	51
VI	1.55	3.9	180	150	19.5	28	31.5

d_0 ... die diameter
L/R ... die geometry (ratio length/radius)
α ... die entrance angle ('flat' die: $\alpha = 180°$)
T ... melt temperature.

Table 20 gives the results for the onset of melt fracture. Both participants IV and VI come to the conclusion that sample A has a lower D_{crit} than B, and B a lower D_{crit} than C. Participant I reports the opposite result; especially at 190°C, it is obvious that according to I, D_{crit} for sample A is higher than for samples B or C. The reason for this discrepancy is not clear at present (note that the die entrance angle α is different). The data of IV seem to indicate a slight dependence of D_{crit} on die length.

* This result cannot be generalized: e.g. Ramsteiner[35] found the onset of melt fracture to occur at the same 'average' true shear stress (determined from pressure gradient) independent of the shape of the cross-sectional area for the very different dies he used (circle, triangle, square, slits of different ratios height/width).

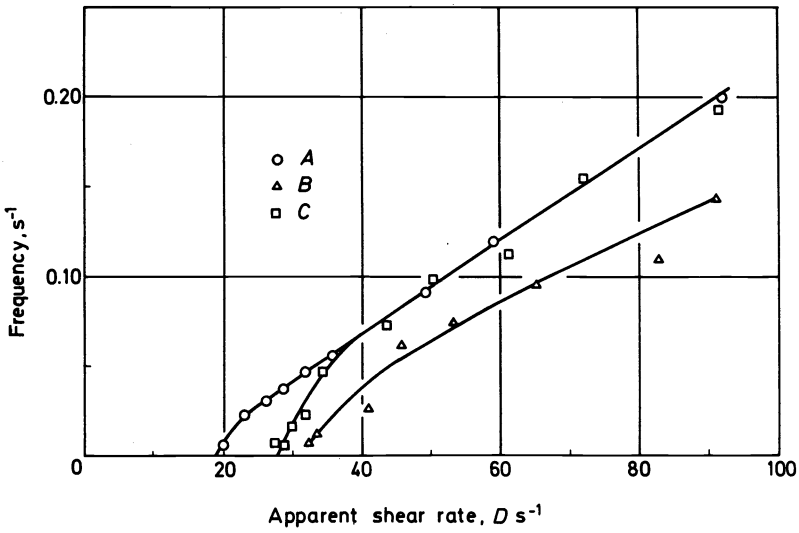

Figure 14. Frequency of entrance flow irregularities (connected with melt fracture) as a function of apparent shear rate D. Capillary extrusion, $d_0 = 1.55$ mm, $L/R = 3.9$, 'flat' die, $T = 150°C$; results from VI. Intercepts of the abscissa give the critical apparent shear rates D_{crit} for the onset of melt fracture.

The flow irregularity data provided by VI are remarkable *per se* (*Figure 14*): in spite of A and C differing in D_{crit}, both samples have the same dependence of the frequency of the flow irregularities on shear rate for $D > 2D_{crit}$. B develops lower frequencies of the irregularities throughout the whole range of shear rates applied.

(C3.5) *Birefringence in the slit viscometer*

In slit extrusion with '1', '2' and '3'-directions denoting the velocity, the gradient and the 'neutral' direction, respectively, transmission of polarized light in the direction '2' enables one to determine the optical path difference P between the two components of the electrical field vector in the directions '1' and '3'*. The ratio $\Phi = P/h$ is correlated with the difference $(n_{11} - n_{33})$ of components of the refractive index tensor n_{ik}. A method for the measurement of Φ was developed by Wales[38] who showed that for fully developed flow

$$\Phi = \frac{P}{h} = \frac{1}{h}\int_{-h/2}^{h/2} (n_{11} - n_{33})\,dy \tag{10}$$

and

$$(n_{11} - n_{33})_w = \Phi[1 + d\ln\Phi/d\ln p_{12,w}] \tag{11}$$

In equation 10, y is the coordinate for the gradient direction '2', and h is the

* A review of flow birefringence of polymer melts is given in ref. 36; for a more general review, see ref. 37. Using the slit viscometer, birefringence measurements can be performed at higher shear rates than in the cone-and-plate rotational viscometer.

thickness of the slit. Equation 11 is similar to the formula for the Rabinowitsch correction[20] in capillary flow: the quantity investigated is referred to the wall of the slit and connected with the measured signal Φ and its (logarithmic) derivative with respect to shear stress. The suffix w denotes the wall value.

Because of the stress-optical law, $(n_{11} - n_{33})$ is a measure for the normal stress difference $(p_{11} - p_{33})$ connected with the shear flow. The validity of the stress-optical law for polymer melts has been demonstrated recently for the conditions of steady shearing flow[39]. For the comparison of birefringence for the three samples A, B and C, the comparison of the directly measured quantity Φ and its dependence on apparent shear rate D seems to be sufficient. Φ depends also on 'flow history'; therefore, the value L of the path length at which the optical measurements were made was varied.

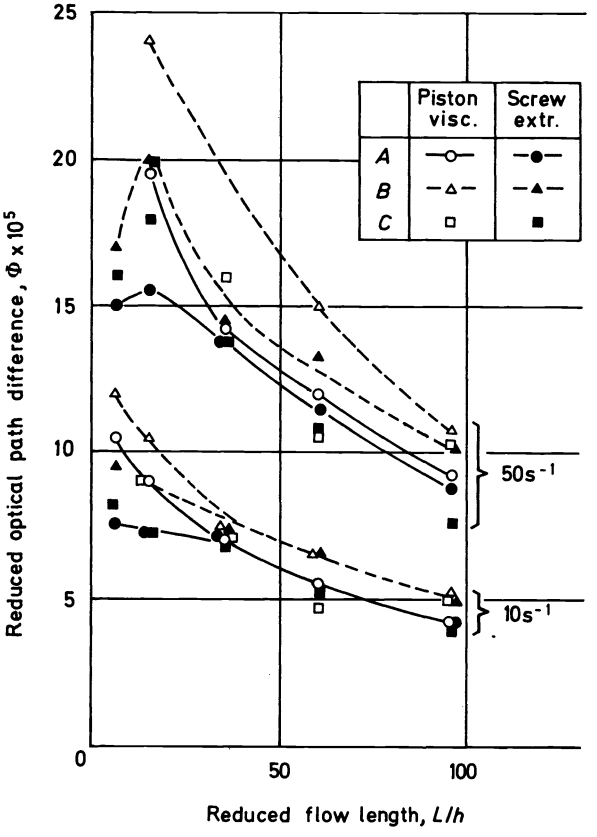

Figure 15. Reduced optical path difference $\Phi = P/h$ as a function of reduced flow length L/R in slit extrusion at constant apparent shear rate D_s, $T = 150°C$; results from VI. The points represent averages from replicate measurements.

The measurements were performed at 150°C using two methods of feeding the slit: (a) the pressure system and the cylinder of a piston viscometer, and

(b) a screw extruder. *Figure 15* gives an example for the dependence of the 'reduced optical path difference' $\Phi = P/h$ on 'reduced flow length' L/h for two constant apparent shear rates $D_s = 6q/wh^2$ (q denotes volume output rate; w is the width; h is the height of the rectangular cross section of the slit; L denotes the distance from the slit entrance). Φ decreases enormously with increasing L/h. Clearly, conditions of fully developed flow cannot easily be obtained with these polymer melts.

With equation 10 and the stress-optical law, it follows from this result that, in slit extrusion, the normal stress difference $p_{11} - p_{33}$ must relax during flow and consequently that there must be a retardation of the corresponding recoverable shear strain during the flow of the polymer melt in the slit. The same conclusion was drawn already from the extrudate swell versus die length data (compare section C3.3).

Figure 15 represents the birefringence data, and shows that the piston viscometer feed and the extruder feed do not give the same results. The extruder gives lower Φ values especially at short distances from the entrance. Possibly, the structure of the polymer melts has been broken down by the shearing action of the screw. However, with respect to the differences in the flow behaviour of the three samples A, B and C, it is clear that sample B always shows a greater birefringence than samples A and C, and that A and C do not differ significantly. This result is valid over the whole shear rate range investigated.

(C3.6) *Appendix to section C3: Measurements with melt indexer at lower temperatures*

The rheology work presented in this paper was mainly performed at 150°C, with a few exceptions: the viscosity function was also measured at 190°C (*Figure 7*), and the temperature dependence of the zero shear viscosity $\eta_0(T)$ was determined (*Table 11*). It was found that in the linear-viscoelastic range, the time–temperature superposition principle was applicable ('thermo-rheological simple fluid'). At different temperatures, the differences in the linear-viscoelastic properties between the three samples are small; it follows that $\eta(T)$ should be nearly the same for A, B and C, provided that the Cox–Merz relation[40] is valid. The validity of this relation for various kinds of polymer melts has been established previously[41].

However, the footnotes on pages 555 and 557 as well as the data for the 'as received' samples of *Figure 2* indicate a very surprising result: measurements in the melt indexer show noticeable differences between the three samples when performed at low temperatures. This result was confirmed by other participants too, as can be seen from *Table 22*: at 125°C, participants I and IV obtained nearly the same absolute data. Sample C shows approximately twice the output rate of sample A, and B is also very different from A. At 150°C, the differences between A, B and C are smaller, but still well pronounced. For 150°C and the same piston load, participant IV reports differences between A, B, and C other than those of participant V.

Because of the similar $\eta_0(T)$ curves and the similar linear-viscoelastic behaviour at different temperatures, the differences between the samples in melt indexer output rate at low temperatures should be attributed to melt elasticity differences at shear rates $\dot{\gamma} > \dot{\gamma}^*$, e.g. to the different temperature

Table 21. Reduced optical path difference Φ in slit die, results from VI. Entries represent the averages of replicate measurements

	Piston viscometer				Screw extruder			
		$\Phi \times 10^{+5}$				$\Phi \times 10^{+5}$		
D_g, s^{-1}	L/h	A	B	C	L/h	A	B	C
1	6	2.6	2.6	—				
	14	2.8	2.9	2.6				
	35	—	2.0	1.95				
2	6	4.0	4.2	—				
	14	4.25	4.3	3.8				
	35	3.5	3.4	3.0				
5	6	6.8	7.6	—	6	5.5	—	(5.8)
	14	6.65	7.25	6.3	14	5.5	—	—
	35	5.2	5.7	5.05				
	60	3.9	4.3	3.2				
	96	2.7	3.4	3.5				
10	6	10.5	12	—	6	7.5	9.5	8.2
	15	9·0	10.5	9.0	14	7.5	—	—
	35	7.0	7.5	7.1	15	7.3	9.0	7.3
	60	5.5	6.5	4.65	35	7.1	7.5	6.9
	96	4.2	5.2	5.0	60	5.2	6.5	5.2
					96	4.2	4.9	3.9
					6	10	12	11
20	15	12.5	14.7	13	14	10	—	—
	35	9.5	9.6	10	15	10.8	13	11
	60	8.0	9.1	6.5	35	9.75	10	9.2
	96	6.0	6.2	7.3	60	7.3	8.9	7.0
					96	5.9	6.3	5.2
50	15	19.5	24	—	6	15	17	16
	35	14.2	—	16	15	15.5	20	18
	60	12	15	10.5	35	13.8	14.5	13.8
	96	9.2	10.8	10.3	60	11.5	13.3	10.8
					96	8.8	10.1	7.6
					15	22	26	24
100	60	16.5	—	—	35	20	19	18.8
	96	13.5	14.8	14.0	60	15	17.3	14.5
					96	11.8	13.8	10.4
200					15	29	34	32
					35	27	24.5	25
					60	21	23.3	20
					96	16	18.2	14
500					35	40	35	—
					60	28	—	30
					96	23	25	20

Table 22. Melt indexer measurements at low temperatures*

(1) Output rate in g/10 min

Participant	T, °C	F, kgf	A	B	C
I	125	8.6	1.35	1.99	2.45
IV	125	8.6	1.36	1.88	2.16
IV	150	5	1.46	2.17	2.48
V	150	2.16	0.30	0.33	0.41
		5	1.26	1.47	1.68
		12	6.72	7.60	9.46
Average (*Table 2*)	190 (standard conditions)	2.16	1.37	1.41	1.59

(2) Melt memory index, per cent*

I	125	8.6	51.5	49.1	44.2
I	190	2.16	51.5	52.7	47.9

* Compare also sections A2 and A3.

dependences of the values of energy density portions II and III (*Figure 9*(a)] for the three samples. However, the melt memory results obtained by I at 125°C do not support this hypothesis, as follows from the lower part of *Table 22*. A further possible explanation could lie in the different thermal stability (compare *Figure 2*). But a conclusive decision concerning this temperature-dependent behaviour can probably be obtained only by extensive measurements of the rheological behaviour at different temperatures. This is outside the scope of the present paper.

(*C3.7*) *Conclusions of section C3*

Concerning the elastic effects in extrusion flow, three main conclusions can be drawn, as follows.

(a) The same type of measurement performed with different apparatuses, or even with the same apparatus but with different dimensions of the capillary die, leads to different values of the quantities measured. This was not the case for the purely viscous properties (viscosity function, see section C2) or for the linear-viscoelastic properties (see section C1).

(b) Those quantities representing the elastic deformation of the streaming melts within the (capillary or slit) dies decrease remarkably with increasing die length.

(c) The differences worked out between the three samples A, B and C, lead to the general statement (exception: birefringence) that the relative differences are higher the lower the shear rate applied.

For the melt temperature 150°C, the differences between A, B and C, can be listed as follows:

(1) *end correction e*

$$\text{For } D < D_{\text{crit}}, \qquad A > B \approx C$$

For $D > D_{crit}$, $\quad A \approx B > C$

(2) *elastic portion e_0 of end correction*

For $D < D_{crit}$, $\quad A > B \approx C$

For $D > D_{crit}$ $\quad A \approx B > C$,

but for $30 < D < 100\,s^{-1}$: $A \approx B \approx C$.

(3) *geometric portion $(\bar{e} - e_0)$ of end correction*

for $\bar{D} = D_0 < D_{crit}$: $A > B \approx C$

(4) *extrudate swell*

low $\dot{\gamma}$; high $\dot{\gamma}$ and long dies: $A > B > C$
high $\dot{\gamma}$ and short dies: $B > A > C$.

(5) *Melt fracture*, onset

$A > B \approx C$ (participant I)

D_{crit}:

$A < B < C$ (participants IV and VI)

melt fracture, frequency of flow irregularities (at $D > 2D_{crit}$)

$A \approx C > B$

(6) *flow birefringence $n_{11} - n_{33}$*

$B > A \approx C$

This list shows that, in general, at 150°C the (stable) melt flow of sample A is connected with the highest elastic deformation. However, there are distinct exceptions: (a) sample B shows a higher extrudate swell than sample A for short dies at $D = 10\,s^{-1}$, and (b) sample B always has the highest birefringence. An explanation for these exceptions cannot be given yet. A further strange result concerns the temperature dependence of the melt indexer output rates, especially the differences between the samples at 125°C. It is noteworthy that these differences can be attributed neither to the temperature dependence of the linear-viscoelastic behaviour and the zero shear viscosity nor to a correspondingly different extrudate swell (melt memory index) at 125°C melt temperature.

(C4) Rheological studies with cone-and-plate rotational rheometers

The cone-and-plate rotational rheometer has the advantage that the same shear rate exists throughout the volume of the specimen under test. From the torque, the shear stress, and from the axial force which tends to separate the cone and the plate, the first normal stress difference $(p_{11} - p_{22})$ can be determined. This is the case in the Weissenberg rheogoniometer[42] and other, more recent instruments, see e.g. ref. 43. In measuring polymer melts, the normal force connected with shear flow can be remarkably high. In addition, it

turns out that, at constant applied shear rate, both quantities recorded, i.e. torque and normal force, are time-dependent, in other words, shear stress p_{12} and first normal stress difference $(p_{11} - p_{22})$ are transients at constant $\dot{\gamma}_0$. Shear stress and first normal stress difference as functions of shear rate and of time are the main subject of the first part of this section*.

The elastic properties connected with shear flow can be characterized not only mechanically but also optically in the cone-and-plate system by means of the experimental method of Wales and Janeschitz-Kriegl[45], whose birefringence studies (with cone-and-plate) are also presented in this section. The relaxation of stress and birefringence after cessation of shear flow and the results of very recent creep tests together with data on creep recovery, give additional information concerning the rheological behaviour of the three melts.

(C4.1) *Dependence of p_{12} and $(p_{11} - p_{22})$ on shear rate*

Participant I measured at 130°C with the commercial version (model R-16) of the rheogoniometer†. The shear rates used were rather low; after an initial stress growth, and sometimes an overshoot, the stresses were reported to attain constant values independent of time.

Table 23. Shear stress and first normal stress difference at 130°C, in 10^4 dynes/cm^2; results from I

$\dot{\gamma}$	A		B		C	
$[s^{-1}]$	p_{12}	$p_{11}-p_{22}$	p_{12}	$p_{11}-p_{22}$	p_{12}	$p_{11}-p_{22}$
0.0043	0.353	—	0.356	—	—	—
0.0085	0.707	—	0.83	—	0.714	—
0.0135	1.11	—	1.21	—	1.02	—
0.0269	1.99	2.13	2·00	2.32	1.85	2.00
0.0425	2.72	3.78	2.92	4.30	2.73	3.93
0.085	4.52	9.66	4.84	9.89	4.40	8.59
0.135	6.00	12.6	6.45	16.2	5.81	14.5
0.269	9.01	25.2	9.36	29.7	9.11	25.7
0.425	11.6	37.1	11.3	38.0	10.9	34.7
0.85	15.6	55.3	15.2	52.7	—	—

These constant values are listed in *Table 23*. The comparison of data for samples A, B and C, can be summarized as follows: the shear stresses are practically the same, the difference between A, B, C being often much less

* The determination of the second normal stress difference $(p_{22} - p_{33})$ by additional normal force measurements of the melts in parallel platens (in rotation) was intended originally. However, because of the non-homogeneous shear rate in the gap of this device, the application of the generally used formula by Kotaka *et al.* does not seem to be applicable if the stress components are not only functions of shear rate but also of time. This formula is used for the calculation of $(p_{22} - p_{33})$ from the normal force and its variation with shear rate at the rim of the gap[44].

† Measurements of I at 190°C showed differences between 'as received' and 'stabilized' samples probably because of lack of thermal stability of the samples, see also section A7. Therefore, only measurements at 130 and 150°C will be discussed here.

than ten per cent. The results for $(p_{11} - p_{22})$ are, on the average, also equal for A and C. Sample B, however, seems to have a slightly higher normal stress difference which differs from that for A by about 0–20 per cent, except at the highest shear rate used by participant I, $\dot{\gamma}_0 = 0.85\ s^{-1}$, at which the normal stress difference for B is lower than that for A. It must be kept in mind, however, that normal force measurements for polymer melts made with the commercial version of the rheogoniometer involve tremendous experimental difficulties. In any case, the rheogoniometer data obtained by I give only a little, if any, difference in the behaviour of the three samples A, B and C.

(C4.2) *Time dependence of* p_{12} *and* $(p_{11} - p_{22})$ *at constant shear rate*

These studies were performed by participant IV using a model R12/15 of the rheogoniometer to which several vital modifications had been made in order to obtain the transient behaviour of polyethylene melts correctly[10]. The measurements were made at 150°C and the constant shear rates $\dot{\gamma}_0 = 0.1$–1–$10\ s^{-1}$. A remarkable time dependence (including the stress growth period) is found for p_{12} and $(p_{11} - p_{22})$. The time-dependent behaviour differs from one shear rate to another, as shown by detailed studies[10] already presented for sample A*.

Table 24. Number of specimens used and bandwidth of the measured functions in the reproducibility tests. The 'bandwidth' refers to the position of the maxima of the functions. Sample A, $T = 150°C$; results from IV

	$\dot{\gamma}_0 = 0.1$	1	$10\ s^{-1}$
Number of specimens	13	8	6
$\Delta p_{12}/p_{12,\max}$ [%]	9	10	7
$\Delta(p_{11} - p_{22})/(p_{11} - p_{22})_{\max}$ [%]	23	11	4

The sometimes small differences found in the rheogoniometer data for A, B and C, raise the question of the reproducibility of the results. For this purpose, the reproducibility was checked with sample A using always a new specimen for each measurement performed under equal experimental conditions. These reproducibility tests result in a remarkably large bandwidth obtained for the transient functions. The reason for this finding is not known at present†. The number of specimens used and the resulting bandwidths for shear stress and normal stress difference (at the maximum of these curves) are listed in *Table 24*. For $(p_{11} - p_{22})$, the bandwidth increases with decreasing shear rate and amounts to 23 per cent at $\dot{\gamma}_0 = 0.1\ s^{-1}$, probably because of the low relative sensitivity of the normal stress-measuring system at this low shear rate. However, the ten per cent bandwidth for shear stress p_{12} is surprisingly high, too.

* As the present publication will expose the differences in the behaviour of A, B, C, the three shear rates selected seem to be sufficient to describe the differences which occur in rheogoniometer flow.

† Possible reasons are: non-concentric insertion of the specimen into the rheogoniometer gap, different thermal prehistory (different resident time at measuring temperature before the measurement starts), problems with the open rim of the filled gap, etc.

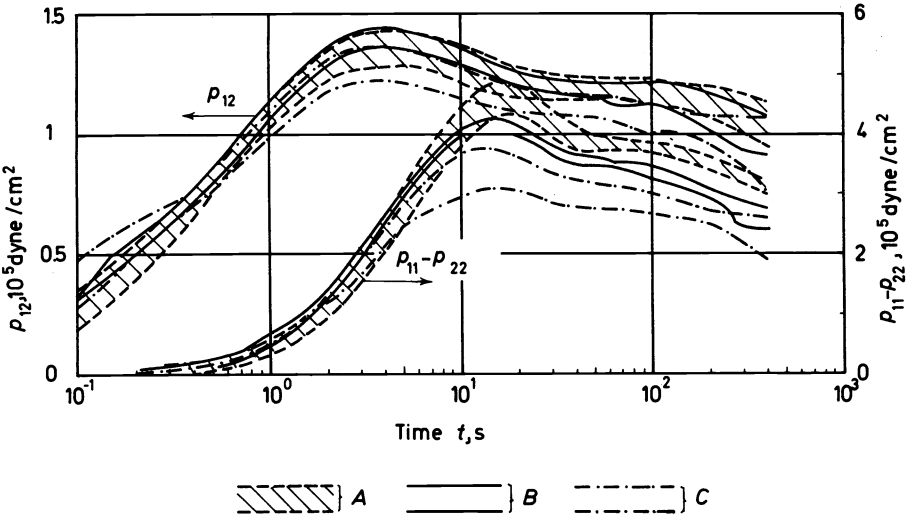

Figure 16. Time dependence of shear stress p_{12} and first normal stress difference $p_{11} - p_{22}$ at constant shear rate $\dot{\gamma}_0 = 1\,s^{-1}$; $T = 150°C$, results from IV. The hatched bands indicate the ranges into which all the curves fall for the eight specimens of sample A. For sample B (four specimens) and C (six specimens) only the bounding curves of the corresponding ranges are drawn (Weissenberg rheogoniometer, platen diameter 24 mm, cone angle 8°).

The time dependence of p_{12} and $(p_{11} - p_{22})$ is shown for $1\,s^{-1}$ shear rate, for all three samples, in *Figure 16*. The general shape of the curves and the magnitude of the bandwidths for repeated measurements are comparable for the three samples. With the hatched band for sample A, the shear stress of B falls within the bandwidth of the curves for A, whereas the normal stress difference of B after the maximum is about 15 per cent smaller when compared with A. Both curves for C are distinctly lower than the curves for A or B. In *Figure 17*, the stress ratio $\Gamma = (p_{11} - p_{22})/p_{12}$ is given as a function of shear strain for the three shear rates used. At $1\,s^{-1}$, the samples differ clearly, with A, B, C in falling order of the magnitude of Γ. The same statement is valid for $0.1\,s^{-1}$ shear rate. It is very interesting, however, that at $10\,s^{-1}$ the Γ curve for B is within the bandwidth for A, and Γ for C is closer to Γ for A or B than at the other two shear rates.

For the three samples the time-dependent functions p_{12}, $(p_{11} - p_{22})$ and Γ differ mostly around the maxima. For a more quantitative discussion, *Table 25* lists the average maxima and in the last two columns the relative difference referred to material C. From this table, the following results can be formulated. (a) The average maxima of the shear stress curves coincide within ten per cent for all the three samples. The maxima of A and B are practically equal and are about six per cent higher than for C. This difference is independent of shear rate. (b) The maxima of $(p_{11} - p_{22})$ show differences which are remarkable with respect to magnitude as well as to their dependence on shear rate. At $10\,s^{-1}$, A and B are equal and differ by about 17 per cent from C. This relative difference increases with decreasing shear rate, and

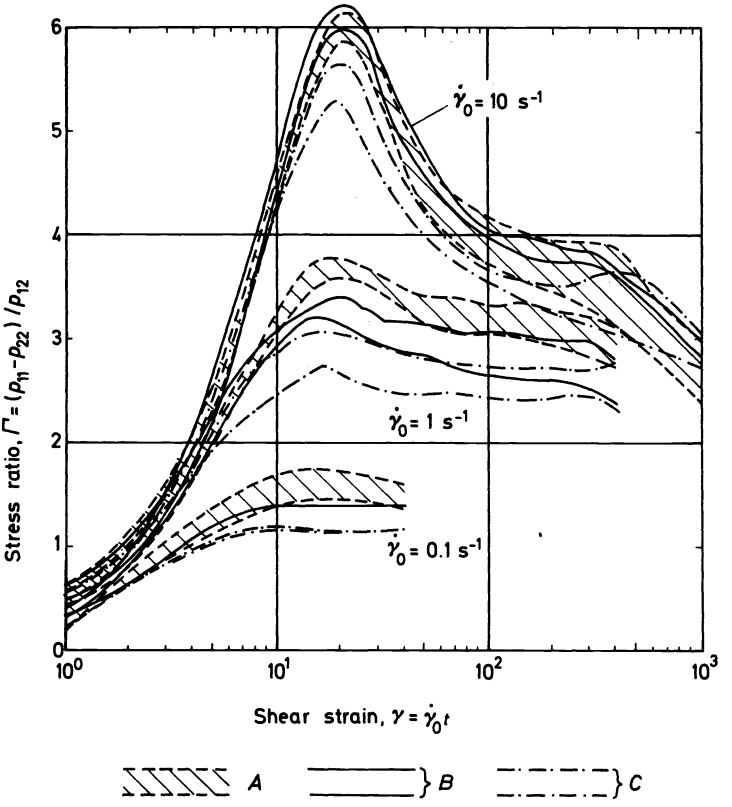

Figure 17. Stress ratio $\Gamma = (p_{11} - p_{22})/p_{12}$ as a function of shear strain $\gamma = \dot{\gamma}_0 t$ for the constant shear rates $\dot{\gamma}_0 = 0.1$–1–10s^{-1}. $T = 150°C$; results from IV. (At $\dot{\gamma} = 0.1\ s^{-1}$, identical functions $\Gamma(\gamma)$ were obtained for sample B from the two tests performed, *Table 25*).

the increase is different for A and B. At 0.1 s^{-1}, $(p_{11} - p_{22})_{max}$ for A is about 40 per cent, and for B about 30 per cent higher than for C. Accordingly, the difference between A and B is only ten per cent. (c) The similar result follows for Γ because of the fact that p_{12} nearly coincides for the three samples.

From the lower part of *Table 25* it follows that the maxima for p_{12} and $(p_{11} - p_{22})$ are approximately located at a constant shear strain $\gamma = \dot{\gamma}_0 t$ independent of shear rate $\dot{\gamma}_0$. For p_{12}, there is practically no difference in $t(p_{12,max})$ between A, B and C. For $(p_{11} - p_{22})$, the maxima occur remarkably late for sample A at the two lowest shear rates.

It is the main result of this section that at all times the shear stress p_{12} is practically equal for A and B. p_{12} is about ten per cent lower for C, whereas clear differences in $(p_{11} - p_{22})$ can be measured around the maxima of these time-dependent functions, provided the shear rate is low enough. This result is particularly interesting because in extrudate swell a similar trend exists (compare section C3.5); in particular, it should be noted that the differences in extrudate swell between A and B increase with decreasing shear rate.

Table 25. Averages of the maxima of p_{12}, $(p_{11} - p_{22})$, and Γ for the three samples A, B, C at different shear rates $\dot{\gamma}_0$, and average occurrence of the maxima. $T = 150°C$; results from IV

$\dot{\gamma}_0$		A	B	C	(A − C)/C[%]	(B − C)/C[%]
0.1 s^{-1}	No. of specimens	13	2	2		
	$p_{12,\max}$ [10^4 dynes/cm^2]	3.04	3.21	2.92	4	10
	$(p_{11}-p_{22})_{\max}$ [10^4 dynes/cm^2]	4.75	4.27	3.32	43	29
	$\Gamma_{\max}$	1.61	1.39	1.18	36	18
1 s^{-1}	No. of specimens	8	4	6		
	$p_{12,\max}$ [10^5 dynes/cm^2]	1.36	1.37	1.29	5	6
	$(p_{11}-p_{22})_{\max}$ [10^5 dynes/cm^2]	4.54	4.14	3.48	30	19
	$\Gamma_{\max}$	3.70	3.28	2.9	28	13
10 s^{-1}	No. of specimens	5	3	3		
	$p_{12,\max}$ [10^5 dynes/cm^2]	4.57	4.41	4.22	8.4	4.5
	$(p_{11}-p_{22})_{\max}$ [10^6 dynes/cm^2]	2.24	2.2	1·9	18	16
	$\Gamma_{\max}$	6.00	6.09	5.49	9	11
0.1 s^{-1}	$t(p_{12,\max})$ [s]	38	38.5	32		
	$t([p_{11}-p_{22}]_{\max})$ [s]	162 (140–190)	105	90		
1 s^{-1}	$t(p_{12,\max})$ [s]	4.3	3.7	3.8		
	$t([p_{11}-p_{22}]_{\max})$ [s]	17	13.8	14.2		
10 s^{-1}	$t(p_{12,\max})$ [s]	0.5	0.52	0.46		
	$t([p_{11}-p_{22}]_{\max})$ [s]	1.7	1.6	1.6		

(C4.3) *Flow birefringence at constant shear rate*

The birefringence measurements in the cone-and-plate system were obtained with the apparatus described in ref. 45. Two quantities were measured: (a) the flow birefringence $\Delta n = n_{\mathrm{I}} - n_{\mathrm{II}}$, which is the difference of the principal values of the refractive index tensor n_{ik} in the flow plane (1–2 plane following the notation of section C3.5); and (b) the extinction angle χ which determines the smallest of the two angles between the optical principal axes and the flow direction in the flow plane. The cone angle of the cone-and-plate rotational system was 1°8′; measurements were performed at 150°C at the constant shear rates $\dot{\gamma}_0 = 0.01$–0.1–1–$10\ s^{-1}$.

Two groups of measurements were made, resulting (a) in steady state birefringence obtained at shear rates $0.01 < \dot{\gamma}_0 < 0.2\ s^{-1}$, and (b) in time-dependent birefringence as a material response to a step function shear rate. *Table 26* gives the steady state birefringence results expressed as Δn and 2χ. It follows from the table that there are no important differences between the data for A, B and C, in general. There is a slightly lower Δn value and a slightly higher 2χ value for B, at least at the lower shear rates used, but the differences involved are less than the errors of the measurements.

At $\dot{\gamma}_0 = 0.1$–1–$10\ s^{-1}$, the time dependence of Δn and χ was determined.

Table 26. Results from birefringence measurements in cone-and-plate system of participant VI: $\Delta n = n_{\mathrm{I}} - n_{\mathrm{II}}$ and 2χ at 150°C

$\dot{\gamma}$ [s^{-1}]	$\Delta n \times 10^6$			2χ [degrees]		
	A	B	C	A	B	C
0.01	2.1	1.8	2.1	72.5	74	72
0.02	3.9	3.2	4.2	65.5	68	67
0.05	8.5	7.6	9.2	56.5	58	57.5
0.1	15.5	15	16	49.5	50	50
0.2	28	27	30	43.5	43.5	43.5

The results are given in *Figure 18**. We note that, for Δn as well as for χ, a transient behaviour is recorded which correlates with the transients of the stress components (compare the preceding section C4.2). However, the often used relation

$$\cot 2\chi = 0.5\Gamma \tag{12}$$

where Γ is the stress ratio $(p_{11} - p_{22})/p_{12}$, is not confirmed quantitatively† This relation follows from the stress-optical law with a scalar as the stress-optical coefficient[37]. A further interesting result from *Figure 18* is that, for one sample and a long duration of the shear test, e.g. $t = 300$ s, the extinction angle χ is larger for $\dot{\gamma}_0 = 10\,s^{-1}$ than for $1\,s^{-1}$. The curves $\Gamma(\gamma)$ do not show the correspondingly lower Γ at $10\,s^{-1}$ (*Figure 17*). However, there is a trend that the Γ values at $\dot{\gamma}_0 = 10\,s^{-1}$ may become smaller than at $1\,s^{-1}$, but only at longer times.

Comparing the three samples, we find that, in the transient tests at $\dot{\gamma}_0 = 0.1\,s^{-1}$, Δn is practically the same for A, B and C. The same result is valid for $\dot{\gamma}_0 = 1\,s^{-1}$, with only slight differences between the three samples. At $\dot{\gamma}_0 = 10\,s^{-1}$, however, Δn for sample B is distinctly larger (up to $\approx$25 per cent) than for A or C, with A and C differing only at short times. The difference in Δn for A and C vanishes with increasing total shear. With respect to χ, it is difficult to work out any difference between A, B and C in the short-time, i.e. the transient region. For $t > 100$ s, sample A definitely has a smaller extinction angle χ at 0.1 and $1\,s^{-1}$ shear rate. At $\dot{\gamma}_0 = 10\,s^{-1}$, the extinction angle of B is slightly smaller than that of A. Assuming that equation 12 is valid, the results of the mechanical measurements (*Figure 17*) do not reflect this correspondingly larger Γ of B. Sample C, however, has a higher angle χ at $10\,s^{-1}$ than either A or B. This is reflected in Γ only at short times.

In summing up, the results of this section show that, following the start of shear flow at constant shear rate, the birefringence measurements give a general transient response of the samples which is similar to that already

* An examination of the experimental reproduciblity was not performed for all shear rates and samples. For C. the bandwidth in Δn was five per cent at $1\,s^{-1}$ and ten per cent at $10\,s^{-1}$. Experimentation was made difficult by the need to wait 20 to 30 minutes between runs to obtain full annealing.

† The results concerning the relation between birefringence and state of stress will be published in a separate paper[46].

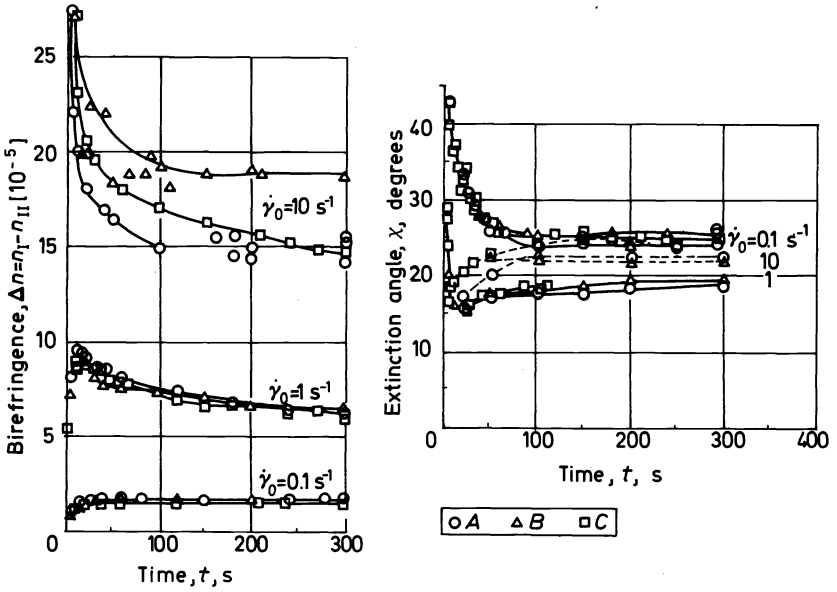

Figure 18. Transient birefringence results as material response to step function shear rate $\dot{\gamma}_0 h(t)$ in cone-and-plate system. Left: $\Delta n = n_I - n_{II}$; right: extinction angle χ; $T = 150°C$, results from VI (Dr Wales).

found from the mechanical measurements. However, the often used equation 12 does not fit the data. At low shear rates, no noticeable difference between the three samples was detected for the equilibrium data. At higher shear rates, the different behaviour of sample B at $\dot{\gamma}_0 = 10\,s^{-1}$ seems to be remarkable: Δn is distinctly higher for B than for A or C, and χ is lowest for B.

(C4.4) *Relaxation of stress and birefringence after cessation of flow at constant shear rate*

At the cessation of flow with constant shear rate, the relaxation of stress (i.e. of p_{12} and $p_{11} - p_{22}$) and of the extinction angle χ were determined by participants IV and VI, respectively. For the mechanical as well as for the optical data, the scatter for repeated tests is rather high, especially at the interesting long times of relaxation. Therefore, definite conclusions concerning the different behaviour for the three samples A, B and C in this type of relaxation test cannot be drawn.

In spite of this difficulty, the following conclusions can be drawn from the data obtained. (a) With increasing magnitude of the preceding shear rate $\dot{\gamma}_0$, the relaxing signals for p_{12}, $p_{11} - p_{22}$, and χ decay more rapidly. For p_{12}, this result was found already by other authors and for other polymer melts[47]. (b) Normal stress differences relax more slowly than shear stresses, as follows from theoretical reasoning[48]. (c) Because of the scatter of the data already mentioned, conclusions to be drawn as to well-established differences in the relaxation behaviour of A, B and C are rather limited. At shear rate $\dot{\gamma}_0 = 0.1$ s^{-1}, A has longer relaxation times than those of B or C, for p_{12}, $p_{11} - p_{22}$,

and χ. A similar statement can perhaps be made at $1\ s^{-1}$, but not at $10\ s^{-1}$ where the relaxation is much more rapid and no significant difference in the relaxation behaviour of the three samples is recorded.

(C4.5) *Creep and creep recovery*

By means of a servo motor drive, shear experiments can be performed with the rheogoniometer under the condition of a constant shear stress p_{12} = constant (creep test), the increase in shear strain $\gamma(t)$, its time derivative $\dot{\gamma}(t)$, and the first normal stress difference $(p_{11} - p_{22})$ being recorded. At the end $(t = t_1)$ of the creep test, p_{12} is quickly brought to zero and kept at zero for $t > t_1$, causing the servo motor to reverse its direction of rotation; this allows one to measure the total (constrained) recoverable shear strain γ_R. For experimental details see ref. 49.

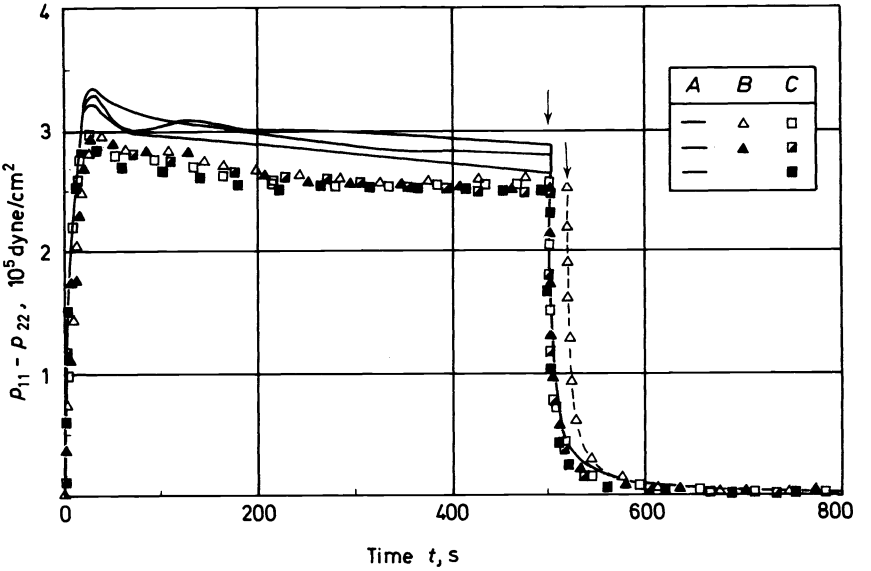

Figure 19. First normal stress difference $(p_{11} - p_{22})$ during creep tests with $p_{12} = 10^5$ dynes/cm^2 for $t < t_1$ (≈ 500 s) and $p_{12} = 0$ for $t > t_1$. t_1 is indicated by an arrow; $T = 150°C$. The measurements were performed in a modified Weissenberg rheogoniometer[49]; results from IV. Different types of points mean different specimens.

In *Figure 19*, the values of $(p_{11} - p_{22})$ for three specimens of sample A, two specimens of B, and three specimens of C are given. The shear stress was kept constant at $p_{12} = 10^5$ dynes/cm^2, and the duration of the creep test was $t_1 = 500$ s. We note a non-constant normal force signal: for each curve after the maximum, there is a steady decrease until a constant value is achieved. Under the conditions of these tests, it is quite clear that sample A has a first normal stress difference which is about ten per cent higher than for B or C; between B and C, no difference is indicated. For samples B and C, the reproducibility of the data is indeed excellent, especially if compared with the reproducibility of the previous data (*Figure 16*). For sample A,

however, some bandwidth still exists*. Numerical data of the test results are given in *Table 27*.

Table 27. Results from creep tests performed with the applied shear stress $p_{12} = 10^5$ dynes/cm^2 (± 1 per cent) = constant during the interval $0 \leqslant t \leqslant t_1 = 500$ s. Total shear strain $\gamma_1 = \gamma(t_1)$, shear rate $\dot{\gamma}_1 = \dot{\gamma}(t_1)$ and stress ratio $\Gamma_1 = \Gamma(t_1)$ obtained at the cessation of the creep flow at t_1. γ_R denotes the total (recoverable) shear strain, and $(p_{11} - p_{22})_{max}$ is the maximum of the first normal stress difference. $T = 150$°C, results from IV.

	A	B	C	Dimension
γ_1	419 427 419	403 397 —	420 449 498	—
$\dot{\gamma}_1$	0.95 1.07 0.91	0.89 0.91 —	1.05 1.03 1.21	s^{-1}
$\Gamma_1 = (p_{11}-p_{22})/p_{12}\|_{t_1}$	2.70 2.84 2.60	2.49 2.49 —	2.56 2.51 2.54	—
γ_R	1.84 1.81 1.80	1.78 1.74 —	1.67 1.66 1.59	—
$(p_{11}-p_{22})_{max}$	3.30 3.28 3.20	2.94 2.92 —	2.94 2.96 2.92	10^5 dynes/cm^2

Table 27 permits one to compare the creep behaviour at the end of the creep tests at $t = t_1 = 500$ s: the total shear γ_1 and shear rate $\dot{\gamma}_1$ are the same, to within ten per cent, for all the specimens of samples A and B. Only sample C shows higher γ_1 and $\dot{\gamma}_1$ values corresponding to a slightly lower viscosity of sample C. In these data for C, some scatter is found for different specimens.

The stress ratio Γ_1 is a little smaller for B than for C, but the recoverable shear strain γ_R is larger for B than for C†. This supports the conclusion already formulated[49] that Γ and γ_R are not proportional, because an assumed factor of proportionality should neither be dependent on material nor depend on the previous flow history; the latter was previously[49] shown not to be the case. Although the differences in the values of Γ/γ_R obtained for A and B are small, we believe they are significant; the scatter in the γ_R data is remarkably low for specimens of the same sample.

* Concerning the reproducibility of the results obtained, it turned out that the results again depend on residence time of the specimens kept at measuring temperature (150°C); if the test was started less than 30 min after the insertion of the specimen into the (pre-heated) gap, the curves of $(p_{11} - p_{22})$ fell within a narrow band, at least for samples B and C.

† Thus the ratio Γ/γ_R depends on the material; it also depends on the total shear strain, as shown previously[49].

(C4.6) *Conclusions of section C4*

At low constant shear rates ($\dot{\gamma}_0 < 1\ s^{-1}$) and 130°C, the measurements of I result in equal values for shear stress p_{12} and first normal stress difference ($p_{11} - p_{22}$) within ten per cent for the three samples A, B and C. Only for sample B some indication of a slightly higher normal force signal is obtained. At $\dot{\gamma}_0 = 0.1$–1–10 s^{-1} and $T = 150$°C, a pronounced time dependence of the signals p_{12} and ($p_{11} - p_{22}$) is found by participant IV. The curves for different specimens of the same sample show a rather broad bandwidth. In these time-dependent functions, practically no difference between A, B and C is found as far as p_{12} is concerned (within ten per cent: A and B have practically the same shear stress; for C, p_{12} is a little lower). With respect to ($p_{11} - p_{22}$), clear differences are found which are highest in their relative magnitude at the lowest shear rate and in the neighbourhood of the maxima: at $\dot{\gamma}_0 = 0.1\ s^{-1}$, $(p_{11} - p_{22})_{max}$ for sample A is about 40 per cent, for B about 30 per cent higher than for sample C.

In birefringence, neither Δn nor extinction angle χ show differences between A, B and C for the steady state flow at low shear rates. At higher $\dot{\gamma}_0 (= 0.1$–1–10 $s^{-1})$, a transient optical behaviour exists. The optical and the mechanical data obtained do not fulfil an often quoted relation derived from the stress-optical law. In contrast to the mechanical results, the most pronounced differences between A, B and C are obtained at higher shear rates, e.g. Δn at $\dot{\gamma}_0 = 10\ s^{-1}$ is 25 per cent larger for sample B than for A or C; A and C differ only slightly. With respect to χ at long shear times $t > 100$ s, A has a smaller extinction angle than B at $\dot{\gamma}_0 = 0.1$ and $1\ s^{-1}$. At $10\ s^{-1}$, χ for B is smaller than for A.

The relaxation results for stress and birefringence after cessation of steady shear flow confirm the results published in the literature concerning the dependence on shear rate. Differences between A, B and C in the relaxation behaviour are not very pronounced: only at $\dot{\gamma}_0 = 0.1$ and $1\ s^{-1}$, has sample A apparently larger relaxation times than B or C; unfortunately, the scatter of these data is very large.

Creep tests (at constant shear stress) have the advantage that the scatter of the results is small when compared with the scatter for tests at constant shear rate. At $p_{12} = 10^5$ dynes/cm^2, the normal stress difference ($p_{11} - p_{22}$) for sample A is about ten per cent higher than for B or C; B and C give the same values for ($p_{11} - p_{22}$). In creep recovery, the recoverable shear strain γ_R can be measured after the cessation of the creep flow. γ_R is largest for A and smallest for C; sample B has only a slightly smaller γ_R than A. Hitherto, Γ and γ_R have been regarded as measures of the 'elasticity' of a melt, and so one might expect them to vary in the same way as we go from B to C. The results show, however, that Γ increases while γ_R decreases.

(C5) Tensile flow properties

When the current test programme was started in 1967, the need for elongational tests in the molten state of the three samples could only be stated, and it was partly because of this need that new experimental methods for the performance of such tests were developed. Much progress has been achieved during the past few years, as can be seen from the review of the current

techniques compiled by Dealy[50]. For the present test programme, two quite different methods were used the results of which are the subject of the following two sections.

(C5.1) *Technical tensile tests*

In order to obtain comparative results for the tensile behaviour of the three melts, a drawdown device is used in connection with a capillary extrusion equipment. The extrudate emerging from the die, is stretched inhomogeneously, and, although the results are of technical interest only, they do reflect interesting differences between the three samples.

With the apparatus of participant I, the extruded, still molten filament passes over a pulley attached to a force-measuring transducer before reaching the variable speed wind-up[51]. Participant IV uses a different technique in so far as use of the pulley is avoided by mounting the variable speed drawdown device on the free end of a leaf spring the bending of which is used for the force measurement[52, 53]. In all these cases, the force is recorded as a function of the drawdown speed. The resulting graph will here be called a 'technical tensile diagram'. The point of break of the filament is of special interest: the maximum force F_{max} represents the 'melt strength', and the maximum drawdown speed or, equally, the maximum rotational speed of the wind-up device, v_{max} or n_{max}, respectively, characterize the 'extensibility' of the melt. During these tests, it was necessary, of course, to keep the output rate of the capillary viscometers constant for the three samples*.

Figure 20 gives examples for the directly recorded technical tensile diagrams, obtained at a melt temperature (in the viscometer barrel) of 150°C. As can be seen from this figure, the diagrams look different for the three samples. Sample A has the highest tensile force ('melt strength') but the smallest extensibility. For sample C the opposite is valid, and B is somehow between A and C. The same statement follows for 150°C from *Table 28* where the average results of more tests are listed together with details of the test conditions. It follows from this table that the differences between the three samples are more pronounced at 150°C melt temperature than at 190°C. Moreover, at 190°C, sample B is rather similar to A with respect to the maximum drawdown speed. Concerning maximum tensile strength, F_{max} is greater for B than for A at 190°C, whereas at 150°C sample A has the highest F_{max}. Sample C has the lowest tensile strength and the highest extensibility under all conditions applied.

It should be pointed out that the technical tensile test is very simple to perform and that its results reflect similarities to the drawdown behaviour of the three samples in film blowing (compare *Table 7*). Similar studies on melt strengths of different types of polymers were performed by Busse[54]. From a more physical point of view, however, this type of test has the disadvantages of inhomogeneous deformation and non-constant temperature field of the specimen under test.

* Participant IV used the simple melt indexer (see section A2) as capillary viscometer at which the piston weight had to be adjusted to maintain a constant output rate. Later a special device was attached to the melt indexer in order to provide a constant piston rate delivering a constant output rate independent of the flow resistance of the melt under test[52].

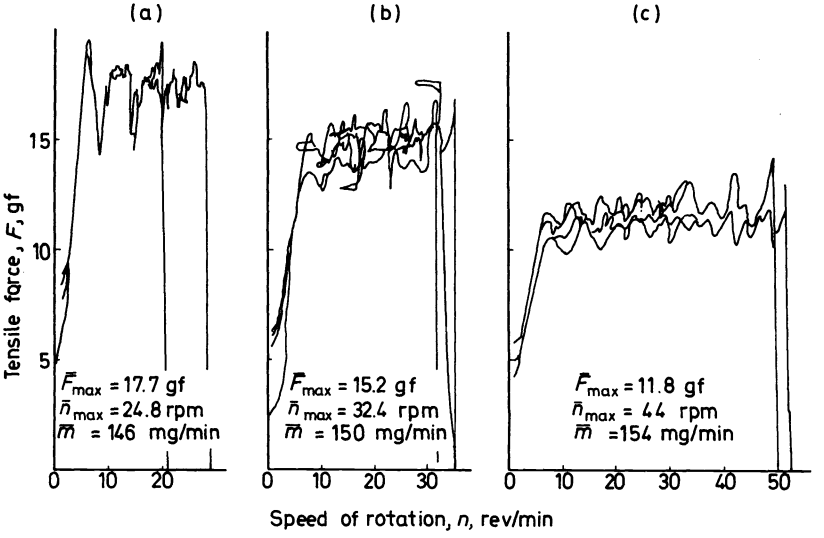

Figure 20. Copy of original records of 'technical tensile diagrams' obtained from tensile tester[52]. For each charge of the viscometer, three diagrams were measured and recorded on the same paper. Melt temperature: 150°C; for further test conditions, see *Table 28*. The speed of rotation of the drawdown device is proportional to the drawdown velocity v of the molten filament. Results from IV.

Table 28. Conditions and average of results of technical tensile tests

Participant		I	IV		Dimension
Capillary length L		50.8	8		mm
Capillary diameter d_0		1.27	2.095		mm
Capillary entrance angle α		90	180 (='flat' die)		degrees
Length of melt extension L'_0		89	50		mm
Melt temperature		190	190	150	°C
Output rate at die		280	145±5	150±5	mg/min
Force at filament break, F_{max}	A	4.6	8.6	17	10^3 dynes
	B	5.2	10.9	14.5	
	C	4.2	8.1	12	
Take-off velocity at break, v_{max}	A	10.2	2.56	3.53	cm/s
	B	10.2	3.01	5.15	
	C	17.8	4.2	6.12	

(C5.2) *Determination of stress/strain relations*

In order to perform tensile tests with a homogeneous deformation of the specimen, two different methods were used: participant I uses an Instron tensile tester with a controlled movement of the crosshead speed such that the Hencky strain rate $\dot{\varepsilon} = \dot{\varepsilon}_0 = \text{constant}$ during the test period. This method was described formerly by Ballman[55] for the performance of tensile

tests of molten polystyrene. The specimen has the form of a dumb-bell whose neck has a diameter of 6.4 mm (0.25 in.) and a length of 12.7 mm (0.5 in.). The specimens are moulded and annealed before the tensile test is started.

Participant IV used a new type of extensional rheometer for polymer melts[52, 56] in which two pairs of gears act as 'rotating clamps'. By avoiding clamping problems, the deformation is homogeneous, and large total strains up to $\varepsilon = \ln \lambda = 4$ can be achieved [λ denotes (length at time t)/(initial length)]. The specimen used by IV is an extruded rod of about 80 cm length which is molten and floating on silicone oil in the apparatus. After melting, the rod shrinks due to a pre-orientation in the rod caused by the extrusion process. After completion of the shrinking, the specimen is clamped into the gears and the stretching operation is performed by rotating the clamping gears in opposite directions with constant speed of rotation. At any chosen point on the stress/strain diagram, the specimen can be cut into little pieces which shrink from the cutting length L_A, between two scissors performing the cutting operation, to the length L_R, after complete recovery. From the equation

$$\varepsilon_R = \ln (L_A/L_R) \tag{13}$$

the recoverable portion ε_R of the total tensile strain ε, obtained at the end of the extensional operation, can be calculated (compare also ref. 53).

Participant I measured at 140°C and obtained a tremendous scatter of the stress/strain relations for different specimens of the same sample. Within this scatter, no distinct differences between the three samples A, B, C can be detected. At low tensile strain rates, samples A and C were difficult to extend to the maximum total strain $\varepsilon = 3$ of I, whereas sample B completed this total tensile strain more easily without rupture. Participant IV noticed also that it was rather easy with sample B to perform these tests without rupture at 150°C and the lowest tensile rate $\dot{\varepsilon}_0 = 0.001\ s^{-1}$. However, at this $\dot{\varepsilon}_0$ value, the duration of a test is rather long and this can lead to a variation in the structure of the melt due to molecular reactions*. In the following, therefore, tests with $\dot{\varepsilon}_0 = 0.001\ s^{-1}$ will not be considered. In *Figure 21*, stress/strain relations for the three samples are given for the strain rates $\dot{\varepsilon}_0 = 0.01$–$0.1$–$1\ s^{-1}$. The temperature of the measurement was 150°C; it should be added that, in general, the reproducibility of the results is good (compare also Figure 4 of ref. 53), except for sample A at 0.01 and sample B at $1\ s^{-1}$. In *Figure 21*, the corresponding hatched areas with the upper and lower limiting diagrams show the range in which stress/strain curves were located in these two cases.

From *Figure 21*, it follows that, for $\dot{\varepsilon}_0 = 0.01$ and $0.1\ s^{-1}$, the stress/strain relations show pronounced differences between the three samples. However, these differences start to develop at total strains of $\varepsilon > 2$, and they are remarkably large for $\varepsilon > 3$. In this region of highest total strain, sample A shows the highest tensile stresses σ, whereas B and C show a relative early flattening of the strain-hardening range of the stress/strain diagram (at

* Compare section A7; with these non-stabilized samples A, B, C at 150°C, a remarkable increase of the stress in the stress/strain relations is observed if the total time t_0 for which the melt stays at measuring temperature is too long. This was checked by applying a different pre-heating time t_0 prior to the start of the measurement.

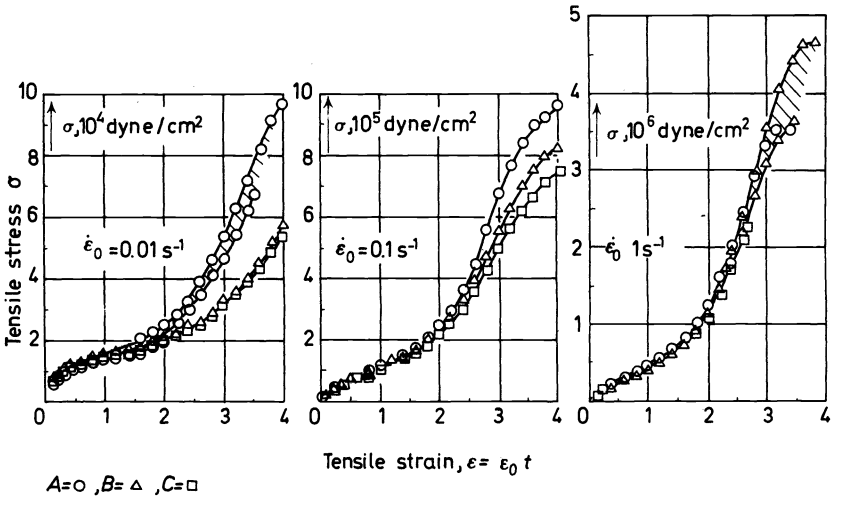

Figure 21. Stress/strain relations $\sigma(\varepsilon)$ obtained from homogeneous elongated test specimens at 150°C melt temperature and different constant strain rates $\dot{\varepsilon}_0$. ε and $\dot{\varepsilon}_0$ are expressed in the Hencky measure; results from IV.

$\dot{\varepsilon}_0 = 0.1\ s^{-1}$), or a later onset of this strain-hardening region (at $\dot{\varepsilon}_0 = 0.01\ s^{-1}$). For the comparison between B and C, it should be noted that, at $\dot{\varepsilon}_0 = 0.1\ s^{-1}$, the curve for B lies between the curves for A and C, whereas, at $\dot{\varepsilon} = 0.01\ s^{-1}$, B and C have identical stress/strain curves. At $\dot{\varepsilon}_0 = 1\ s^{-1}$, however, no difference can be detected between the samples. The curves for A and C fall within (or very near to) the hatched area for sample B. It should be added that, at this tensile rate, not all tests could be performed up to $\varepsilon = 4$ because of rupture of the specimens; e.g., for sample C, three runs gave practically the same stress/strain curve, with a sudden rupture at $\varepsilon \approx 2.6$. Thus a higher total strain than this limit does not seem to be possible with that sample.

It is remarkable that the differences in elongational behaviour of the samples occur at $\varepsilon > 2$ and that they become minor with increasing strain rate $\dot{\varepsilon}_0$. In this context, the results of Chang and Lodge[57] should be quoted: at a total strain $\varepsilon < 1$, the tensile behaviour of a low density polyethylene melt can be described satisfactorily by the rubberlike liquid theory of Lodge[48]. At higher ε, the prediction of the model and the measured behaviour differ, and the difference is smaller the higher the strain rate $\dot{\varepsilon}_0$. This may give an explanation for the behaviour of the samples A, B, C shown in *Figure 21*: if the deviation from the ideal rubberlike liquid behaviour is caused by changes in the structure of the entangled polymer melt network, such changes may be different for the different samples and may be more pronounced at lower strain rates because of the correspondingly increased times of deformation.

The recoverable tensile strain ε_R is listed in *Table 29*. It is surprising that, in general, no differentiation between the three samples can be made, except at $\dot{\varepsilon}_0 = 0.01\ s^{-1}$, where sample B at $\varepsilon > 2$ has about ten per cent smaller ε_R

Table 29. Elastic recovery ε_R after cessation of tensile tests at total (Hencky) tensile strain ε. The tensile tests were performed at constant tensile strain rate $\dot{\varepsilon}_0$ and a temperature of 150°C. Results from IV.

$\dot{\varepsilon}_0[s^{-1}]$	ε	A	B	C
0.001	1	0.17	0.15	0.15
	2	0.22	0.22	0.23
	3	0.29	0.31	0.33
0.01	1	0.38	0.36	0.28–0.34
	2	0.70	0.60	0.50–0.67
	3	1.0	0.87	0.72–0.98
	4	1.24	1.14	0.94–1.24
0.1	1	0.64	0.66	0.63
	2	1.2	1.21	1.15
	3	1.66	1.71	1.60
	4	1.88	1.91	1.76
1	1	0.83	0.84	0.87
	2	1.62	1.61	1.61
	3	2.12	2.28	(2.17)
	4		(2.38)	

values than A. Unfortunately, the results of C at this tensile rate are associated with a large scatter.

(C5.3) *Conclusions of section C5*

The simple drawdown test of a molten filament of samples A, B, C being extruded out of a viscometer die provides differences in the tensile behaviour which correlate with the differences in the film blowing process: sample A has a much higher melt strength and a lower maximum drawdown speed (at which the filament breaks) than has sample C. The behaviour of sample B depends on melt temperature: for the melt strength at 190°C, A < B; for 150°C, the opposite is valid (A > B). Higher melt strength and lower melt extensibility are not directly connected, as follows from the technical tensile diagrams measured at different melt temperatures: at both temperatures, 150 and 190°C, the same order A, B, C exists for increasing melt extensibility of the three samples.

Stress/strain relations $\sigma(\varepsilon)$ measured at constant tensile strain rate $\dot{\varepsilon}_0$ at 150°C also show differences between A, B, C, but only at large total strains ($\varepsilon > 2$) and at relatively low strain rates: at $\dot{\varepsilon}_0 = 0.01\ s^{-1}$, sample A has a value of stress σ which is much higher (at these large total strains) than the values for B and C, which are nearly equal. At $\dot{\varepsilon}_0 = 0.1\ s^{-1}$, the difference between A and B or C is smaller, and at $\dot{\varepsilon}_0 = 1\ s^{-1}$, the difference is practically zero. In spite of these differences in the stress/strain relations, the recoverable tensile strain values ε_R do not differ markedly between the three samples, even at low strain rates.

(D) FINAL RESULTS AND CONCLUSIONS OF THE COLLABORATIVE STUDY

One main objective of the study is the presentation of comprehensive melt

rheology data which were obtained under practically every test condition available at present (except measurement of the temperature dependence of the non-linear viscoelastic properties which were mainly determined at 150°C only). The results of the melt rheology measurements are accurate and reproducible (for one material and the same measurement) within an order of magnitude of ten per cent. This is remarkably good considering the very different types of measurements performed.

For this research programme, the three samples A, B and C were selected in such a way that no differences appear in the usual characterization procedure for LDPE products (however, light scattering faintly indicates that sample A has a small portion of molecules with a very high molecular weight). Likewise, melt rheology yields indistinguishable behaviour for the three samples if:

(*a*) the deformation is in the linear viscoelastic range, or
(*b*) the viscosity function (flow curve) is measured.

However, there are differences in the technological behaviour of the three samples which are not reflected by the above-mentioned characterization, and there are also differences to be found in melt rheology:

(*c*) In shear flow, these differences are connected with melt elasticity in the non-linear viscoelastic range. It is remarkable that the (relative) differences are the higher the lower the shear rate, e.g. at 0.1 s^{-1} shear rate, the difference in $(p_{11} - p_{22})$ between samples A and C is about 40 per cent!

(*d*) In elongational flow, differences between A, B and C occur at large total strains only, and (as in shear flow) are more pronounced at low strain rates.

The conclusion which follows immediately from (*a*) to (*d*) is that the behaviour in linear viscoelastic flow does not unambiguously reflect the behaviour in non-linear viscoelastic flow.

The samples A, B, C differ in film blowing (maximum production speed), and these differences correspond to the different elongational behaviour of the melts. The higher stresses in elongation of sample A lead to an earlier rupture and therefore to a lower extensibility of melt A. The 'technical tensile tests' support this conclusion, which is only qualitative. Before quantitative conclusions can be drawn, further investigation is needed, perhaps along the following lines: (a) a more quantitative description of the film blowing process should be used to see whether the large differences in elongational behaviour of the three samples at low strain rates and large total strains are indeed important; (b) the determination of the quantities representing the processing behaviour (e.g. maximum film drawdown) should be improved so as to be comparable in accuracy and reproducibility with the melt rheology data, for example the critical drawdown condition should be determined by means of a continuously variable and not a stepwise variable drawdown equipment; (c) there is still a need for information concerning the application of the results obtained in uniaxial elongation to the multiaxial extension problem of film blowing; (d) not only a rheological but also a thermal analysis of the film blowing process should be made.

The three samples differ remarkably in the optical quality of blown films, due to differences in surface roughness. One might conclude that the formation of the rough surface is connected with the elastic (recoverable) deformation in shear and elongation. In shear flow, appropriate differences do in fact exist between the three samples (e.g. in extrudate swell and in creep recovery), but the recoveries after elongational flow are not very different. Furthermore, the comparison of the extrudate swell of samples A and B may lead to opposite conclusions depending on the length of the extrusion die and the shear rate used. Here again, the need for a more quantitative description of the film blowing process must be pointed out.

The following additional results are of interest. (a) The impact strength for films deformed in the transverse direction of the film production is less for sample B than for A or C. (b) Flow irregularities in the melt fracture region in capillary flow occur with the same frequency for samples A or C, but they have a lower frequency for sample B. (c) The birefringence of sample B is always highest, in capillary as well as in cone-and-plate flow (at higher shear rates). (d) Melt indexer output rates are very different for A, B and C at a low melt temperature (125°C). (e) The stress ratio Γ and the constrained recoverable shear strain γ_R for the three samples show differences which do not correlate with each other. All these observations call for more fundamental studies.

During and because of the performance of this test programme, new experimental methods were developed or improved. In several aspects, polymer melt rheology data are published here which are not commonly measured: (1) birefringence and extinction angle in shear flow, (2) transient behaviour of the first normal stress difference in shear flow at constant shear rate, (3) in shear flow: creep and creep recovery including normal stress measurements, (4) frequency of flow instabilities in extrusion flow in the melt fracture region, (5) tensile data. The results obtained demonstrate that these new types of measurements provide reasonable and reliable information. On the other hand, the data also show that for LDPE, especially when measured at temperatures above 150°C, the instability of the melts may become a serious problem for experimenters.

Probably the most important result of this collaborative work is the proof that members from different, even competing, companies can cooperate in order to study and discuss problems of common interest. The participating members of the IUPAC Working Party on Structure and Properties of Commercial Polymers believe that this paper is a further realistic contribution to the question of the 'reasonable' characterization of polymers and to the question of the correlation between parameters representing the structure and those representing the physical as well as the technological properties of the processing and the end-use behaviour.

The lengthy collaborative investigations described in this paper have yielded conclusions of considerable importance to the plastics industry; have raised, or re-emphasized, a number of questions still requiring answers; and, finally, have furnished an extensive and varied compilation of reliable experimental data which, it is to be hoped, will provide a stimulating basis for further theoretical investigations (in the universities, in particular) which could perhaps answer these questions. The data were obtained, not from model

substances, but from industrially important products and grades which the polymer engineer has to handle every day.

REFERENCES

[1] J. L. S. Wales, *Pure Appl. Chem.* **20**, 331 (1969).
[2] T. S. Lee, *J. Appl. Polymer Sci.* **13**, 395 (1969).
[3] International Standard *ISO 1872* (1972).
[4] C. Strazielle and H. Benoit, *Pure Appl. Chem.* **26**, 451 (1971).
[5] Macromolecular Division of IUPAC, Working Party on 'Molecular Characterization of Commercial Polymers', Meeting on 12 March 1971 at Strasbourg.
[6] A. Rudin and H. P. Schreiber, *SPE Journal*, **20**, 533 (1964).
[7] T. Fujiki, *J. Appl. Polymer Sci.* **15**, 47 (1971).
[8] A. Jobling and J. E. Roberts, *J. Polymer Sci.* **36**, 421 (1959).
[9] A. Kepes, *J. Polymer Sci.* **22**, 409 (1956).
[10] J. Meissner, *J. Appl. Polymer Sci.* **16**, 2877 (1972).
[11] R. A. Mendelson, *Polymer Engng. Sci.* **8**, 235 (1968).
[12] J. Meissner, *Proceedings* of the Fourth International Congress on Rheology, Providence 1963, Part 3, p 437. Interscience: New York (1965).
[13] V. Semionow. *Advanc. Polymer Sci.*, **5**, 387 (1968).
[14] H. Giesekus, *Proceedings* of the Fourth International Congress on Rheology, Providence 1963, Part 3, p 15. Interscience: New York (1965).
[15] N. W. Tschoegl, *Kolloidzschr.* **174**, 113 (1961).
[16] Technical information from Contraves AG, Zürich, Switzerland.
[17] J. L. den Otter, *Rheol. Acta*, **8**, 355 (1969).
[18] F. Schwarzl and A. J. Staverman, *J. Appl. Phys.* **23**, 838 (1952).
[19] J. D. Ferry. *Viscoelastic Properties of Polymers*, 2nd ed. Wiley: New York (1970).
[20] E. Eisenschitz, B. Rabinowitsch and K. Weissenberg, *Mitt. Dtsch. MatPrüfAnst. Sonderheft 9*, 91 (1929).
[21] E. B. Bagley, *J. Appl. Phys.* **28**, 624 (1957).
[22] E. H. Merz and R. E. Colwell, *ASTM Bull. No. 232*, 63 (September 1958).
[23] J. Meissner, *Materialprüfung*, **5**, 107 (1963).
[24] W. Philippoff and F. H. Gaskins, *Trans. Soc. Rheol.* **2**, 263 (1958).
[25] J. Meissner, unpublished results.
[26] A. Ya. Malkin, B. V. Yarlykov and G. V. Vinogradov, *Rheol. Acta*, **9**, 329 (1970).
[27] J. Meissner, *Kunststoffe*, **57**, 702 (1967).
[28] J. Meissner, *Kunststoffe*, **57**, 397 (1967).
[29] R. S. Spencer and R. E. Dillon, *J. Colloid Sci.* **3**, 163 (1948).
[30] A. B. Metzner, E. L. Carley and I. K. Park, *Modern Plastics*, 133 (July 1960).
[31] T. Arai and H. Aoyama, *Trans. Soc. Rheol.* **7**, 333 (1963).
[32] E. B. Bagley, S. H. Storey and D. C. West, *J. Appl. Polymer Sci.* **7**, 1661 (1963).
[33] A. V. Tobolsky and K. Murakami, *J. Polymer Sci.* **40**, 443 (1959).
[34] J. P. Tordella, *Rheol. Acta*, **1**, 216 (1958).
[35] F. Ramsteiner, *Kunststoffe*, **61**, 943 (1971).
[36] J. L. S. Wales and H. Janeschitz-Kriegl, *Kolloidzschr. u.Z. Polymere*, **250**, 1142 (1972).
[37] H. Janeschitz-Kriegl, *Advanc. Polymer Sci.* **6**, 170 (1969).
[38] J. L. S. Wales, *Rheol. Acta*, **8**, 38 (1969).
[39] J. L. S. Wales and W. Philippoff, *Rheol. Acta*, **12**, 25 (1973).
[40] W. P. Cox and E. H. Merz, *J. Polymer Sci.* **28**, 619 (1958).
[41] J. L. S. Wales and J. L. den Otter, *Rheol. Acta*, **9**, 115 (1970).
[42] K. Weissenberg, *The Testing of Materials by Means of the Rheogoniometer*, Farol Research Engineers: Bognor Regis, Sussex, UK (1964).
[43] M. Macosko and J. M. Starita, *SPE Journal*, **27**(11), 38 (1971).
[44] T. Kotaka, M. Kurata and M. Tamura, *J. Appl. Phys.* **30**, 1705 (1959).
[45] J. L. S. Wales and H. Janeschitz-Kriegl, *J. Polymer Sci.* A-2, **5**, 781 (1967).
[46] J. L. S. Wales and J. Meissner, in preparation.
[47] G. V. Vinogradov and A. Ya. Malkin, *J. Polymer Sci.* A-2, **4**, 135 (1966).

[48] A. S. Lodge, *Elastic Liquids*, Academic Press: New York (1964).
[49] J. Meissner, *Rheol. Acta*, **14**, 201 (1975).
[50] J. M. Dealy, *Polymer Engng Sci.* **11**, 433 (1971).
[51] E. J. Kaltenbacher, C. B. Howard and H. D. Parson, *TAPPI*, **50**, 20 (1967).
[52] J. Meissner, *Trans. Soc. Rheol.* **16**, 405 (1972).
[53] J. Meissner, *Rheol. Acta*, **10**, 230 (1971).
[54] W. F. Busse, *J. Polymer Sci.* A-2, **5**, 1249 (1967).
[55] R. L. Ballman, *Rheol. Acta*, **4**, 137 (1965).
[56] J. Meissner, *Rheol. Acta*, **8**, 78 (1969).
[57] H. Chang and A. S. Lodge, *Rheol. Acta*, **11**, 127 (1972).